SAW Filter Analysis in the Quasi-Static Approximation: Theory and Algorithms

Author:

Alexander S. Rukhlenko, Dr.

Web: https://intrasaw.com E-mail: rukhlenko@intrasaw.com

May, 2000

CONTENTS

INTRODUCTION

About the Author

Dr. Alexander S. Rukhlenko received his degree in Radiophysics and Electronics (with distinction) from the Belarusian State University, Minsk in 1978. He received the Ph. D. degree from the Minsk Radio Engineering Institute in 1989. From 1980 to 1993, he worked in the laboratory of Acousto- and Optoelectronics at the Minsk Radio Engineering Institute, where he was responsible for research and development of SAW devices and their applications to signal processing. In 1993, he joined Semiconductor Physics Department at the Belarusian State University to continue his SAW research. Currently, he is a Principal Researcher at the Belarusian State University where he is a head of the SAW devices group.

Dr. A.S.Rukhlenko is one of the recognized world specialists in the field of SAW devices computer-aided design. His research work is known and appreciated abroad. Since 1987, he has contributed a lot to the theory and practice of the computer-aided design of SAW filters based on the IBM PC compatible platform. His state-of-the-art computer-aided design of SAW filters was demonstrated to and highly appreciated by the world-recognized SAW experts. Some parts of his software were purchased and used by the industrial SAW companies.

In 1995, he became a winner of the SAW filter design competition organized among SAW research groups and specialists of the former USSR by the American company SAWTEK, Inc. which is one of the global leaders in SAW design and production. In 1995-1996, he worked with SAWTEK as a SAW consultant for 18 months including 6 months stay in the USA. He stayed for 3 months at the Technical University of Munich, Department of Microwave Engineering as a visiting scientist in 1995. He worked as an invited SAW designer for LG Company, Seoul, South Korea in 1997-1998 where he has been engaged in designing SAW IF filters for mobile communications (CDMA, PCS, etc.). He visited with lectures on the computer-aided design of SAW filters number of the American companies (SAWTEK, Toko of America, Andersen Labs.). In 1999-2000, he took part as an independent contractor and consultant in several cooperative projects with foreign SAW companies.

His present scientific interests comprise computer-aided design of SAW devices, problems of analysis, synthesis, and simulation of SAW filters, design techniques of low-loss IF and RF filters, etc. He has more than 40 publications on acoustoelectronics. Some principal results were presented at the IEEE Frequency Control Symposium (1992, 1993), IEEE Ultrasonics Symposium (1994, 1995), World Congress on Ultrasonics (1995), and in the international periodicals.

How This Book Is Organized

Chapter 1 provides a brief overview of the mixed scattering matrix (*P*-matrix) theory. Its properties and applications to SAW transducer and SAW filter analysis based on the three-port representation of SAW transducers are discussed. The number of the independent *P*-matrix elements is determined and their physical meaning is explained. As a particular case, the mixed scattering matrix of a SAW transducer is deduced in the quasi-static approximation, with its properties discussed. The relationship between the mixed scattering and transmission matrices of a SAW transducer is deduced. An important particular case of the scattering and transmission matrices in the quasi-static approximation completes consideration.

Chapter 2 discusses the properties and calculation of the acoustoelectric (electroacoustic) conversion function of unapodized and apodized periodic SAW transducers in the quasi-static approximation. The basic equations for the acoustoelectric conversion function are deduced in terms of

finger potentials and gap voltages. The results are generalized to the case of the apodized SAW transducers.

Chapter 3 provides the theory of admittance calculation for periodic SAW transducers based on the concept of a nodal admittance matrix in the quasi-static approximation. Closed-form formulae for admittance calculation comprising acoustic conductance and susceptance are deduced for unapodized and apodized SAW transducers. The physical meaning of the deduced closed-form equations is explained. It is shown that equations are simplified in terms of the gap (finger overlap) taps rather than finger length taps.

Chapter 4 continues with a discussion of SAW transducer admittance calculation where the problem of the static capacitance calculation for transducers with arbitrary finger polarities is considered. The closed-form equations in terms of the interelectrode capacitors are deduced which are applicable to both unapodized and apodized SAW transducers. The electrostatic end effects are supposed to be negligible due to the special guard fingers at the both ends of a finite length SAW transducer.

Chapter 5 discusses properties and models of SAW multistrip couplers (MSC), with the basic assumption of two rectangular orthogonal modes with symmetric and antisymmetric amplitude distribution propagating in the MSC (two-mode approach). The solutions for these modes are obtained using several known techniques, particularly:

1) quasi-static approximation (neglecting SAW reflections near the synchronous frequency);
2) reflective array model (RAM) based on the closed-form cascading of the elemental reflective cells;
3) coupling-of-modes (COM) analysis;
4) field approach based on the closed-form equations for the fundamental and first backward space harmonics.

The MSC analysis is completed by calculation of the MSC scattering matrix in terms of the modal scattering parameters.

In Chapter 6, SAW filter modeling is discussed for in-line and dual-track SAW filters based on the closed-form cascading (in the quasi-static approximation) or direct cascading of the constituent scattering matrices. Given the scattering matrices of the SAW filter components (SAW transducers and multistrip coupler if necessary), the overall **Y**-matrix of the SAW filter is found. The two-port **Y**-matrix is converted to the scattering matrix (**S**-matrix) using the relationship of the acoustic and electric variables at the input and output ports of a SAW filter.

1. MIXED SCATTERING MATRIX AND ITS PROPERTIES

1.1. Three-Port Representation of a SAW Transducer

In many practical cases, a SAW transducer can be considered as a reciprocal lossless three-port network with two acoustic ports 1, 2 and one electric port 3 (Fig. 1.1) where the acoustic variables a_i, b_i, i=1,2 denote amplitudes of the incident (incoming) and reflected (outcoming) waves at the acoustic ports and the electric variables I, V are the transducer terminal current and the voltage applied to the transducer bus-bars, respectively.

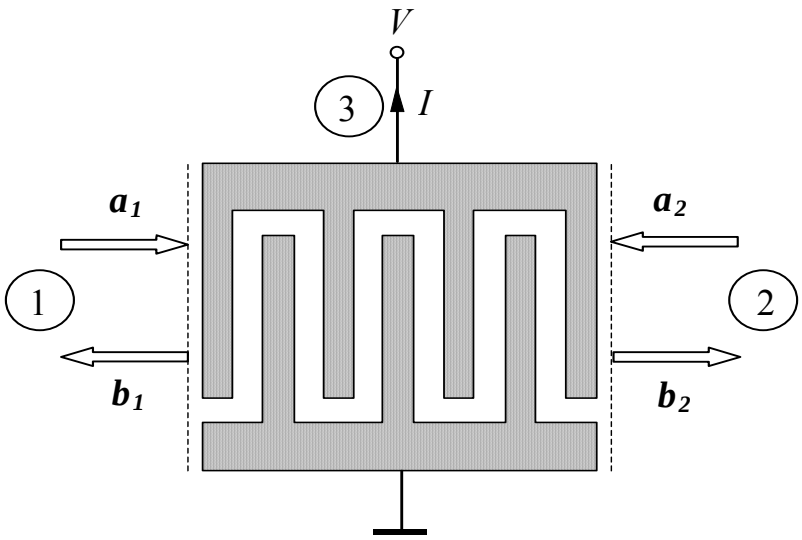

1, 2 – acoustic ports, 3 – electric port

Fig. 1.1. Three-port representation of a SAW transducer

It is convenient to characterize a SAW transducer as a three-port device by its mixed scattering matrix (P-matrix) [1, 2] which is the most closely related with SAW transducer physics. This matrix is a combination of the dimensionless wave scattering coefficients with the mixed units terms to account for acoustoelectric interaction. The matrix relates two reflected wave amplitudes b_i, i=1, 2 and the terminal current I with the incident wave amplitudes a_i and the applied voltage V as follows

$$\begin{bmatrix} b_1 \\ b_2 \\ I \end{bmatrix} = \begin{bmatrix} m_{11} & m_{12} & m_{13} \\ m_{21} & m_{22} & m_{23} \\ m_{31} & m_{32} & m_{33} \end{bmatrix} \begin{bmatrix} a_1 \\ a_2 \\ V \end{bmatrix} \tag{1.1}$$

or in the block-matrix form

$$\begin{bmatrix} \mathbf{B} \\ I \end{bmatrix} = \begin{bmatrix} \mathbf{M_{aa}} & \mathbf{M_{ae}} \\ \mathbf{M_{ea}} & M_{ee} \end{bmatrix} \begin{bmatrix} \mathbf{A} \\ V \end{bmatrix} \tag{1.2}$$

where $\mathbf{A}=[a_1\ a_2]^T$ is vector of the incident waves and $\mathbf{B}=[b_1\ b_2]^T$ is vector of the reflected waves at the acoustic ports. The acoustic matrix-block $\mathbf{M_{aa}}=[\ m_{ik}]$, i,k=1,2 describes scattering properties of a short-

circuit SAW transducer (passive grating, V=0). The acoustoelectric matrix-block $\mathbf{M}_{ae}=[\,m_{13}\,m_{23}]^{T}$ characterizes SAW excitation (acoustoelectric conversion) by a SAW transducer with the voltage V applied to the transducer bus-bars. The electroacoustic matrix-block $\mathbf{M}_{ea}=[\,m_{31}\,m_{32}]$ gives a contribution to the terminal current I induced by the incident acoustic waves. Finally, the electric term $M_{ee}=[m_{33}]$ corresponds to the transducer admittance $Y=m_{33}$.

By definition, the matrix elements $m_{ii}=b_i/a_i$ and $m_{ik}= b_i/a_k$, i,k=1,2 are the reflection and transmission coefficients of a short-circuit transducer (V=0). The elements $m_{i3} = b_i/V$, i=1,2 are the acoustoelectric conversion functions (in SAW excitation mode) in the left and right directions, respectively. By analogy, the terms $m_{3i} = I/a_i$, i=1,2 are the electroacoustic conversion functions (in SAW detection mode) from the left and right directions. The element $m_{33}=Y=I/V$ is the transducer admittance seen at the electric port when there are no incident waves at the acoustic ports (**A**=**0**).

At each port (either acoustic or electric) we can define the following relationship between the electrical variables and generalized wave amplitudes [3]

$$\begin{cases} I_k = \sqrt{Y_k}\,(a_k - b_k) \\ V_k = \sqrt{Z_k}\,(a_k + b_k) \end{cases} \tag{1.3}$$

and the inverse relation

$$\begin{cases} a_k = \dfrac{1}{2}(\sqrt{Y_k}V_k + \sqrt{Z_k}I_k) \\ b_k = \dfrac{1}{2}(\sqrt{Y_k}V_k - \sqrt{Z_k}I_k) \end{cases} \tag{1.4}$$

where a_k, b_k are the amplitudes of the incident and reflected waves, I_k, V_k are the current and voltage, and $Z_k=1/Y_k$ is the characteristic impedance at the k-th port. According to Eq. (1.3) the average power delivered to the k-th port is

$$P_k = \frac{1}{2}\mathrm{Re}\left\{V_k I_k^*\right\} = \frac{1}{2}\mathrm{Re}\left\{\left|a_k\right|^2 - \left|b_k\right|^2 + (a_k^* b_k - a_k b_k^*)\right\} = \frac{1}{2}\left(\left|a_k\right|^2 - \left|b_k\right|^2\right) \tag{1.5}$$

as the quantity ($a_k^{*}\,b_k$ - $a_k b_k^{*}$) is purely imaginary. By other words, the average power delivered through the k-th port is equal to the power of the incident wave minus the power of the reflected wave. It is worthy to note that this definition of the mixed scattering matrix is more physical and convenient for practical use if compared to those given in [1, 2].

Following our definition of the mixed scattering matrix, the acoustic matrix elements m_{ik}, i,k=1,2 are dimensionless, the acoustoelectric conversion elements (mixed units) m_{i3}, m_{3i}, i=1,2 have the units $\sqrt{A/V}=1/\sqrt{\Omega}$, and the electric port admittance m_{33} has the units Ω^{-1}.

1.2. Mixed Scattering Matrix Properties

The basic properties of the mixed scattering matrix **M** can be deduced from the known properties [3] of the wave scattering matrix **S**. By substitution of Eq. (1.3) applied to the electric port 3 into Eq. (1.1) we obtain the dimensionless wave scattering matrix $\mathbf{S}=[s_{ik}]$, i,k=1,2,3 which relates the amplitudes of the reflected and incident waves at all three ports

$$\mathbf{B} = \mathbf{SA} \tag{1.6}$$

where $\mathbf{A}=[a_1\ a_2\ a_3]^{\mathrm{T}}$ is vector of the incident waves, $\mathbf{B}=[b_1\ b_2\ b_3]^{\mathrm{T}}$ is vector of the reflected waves. With help of Eqs. (1.1)-(1.4), the matrix blocks of the wave scattering matrix **S** can be expressed in terms of the appropriate matrix blocks of the mixed scattering matrix **M** as follows

$$\mathbf{S}=\begin{bmatrix}\mathbf{S}_{aa} & \mathbf{S}_{ae}\\ \mathbf{S}_{ea} & \mathbf{S}_{ee}\end{bmatrix}=\begin{bmatrix}\mathbf{M}_{aa}-\dfrac{\mathbf{M}_{ae}\mathbf{M}_{ea}}{Y_0+Y} & 2\dfrac{\sqrt{Y_0}}{Y_0+Y}\mathbf{M}_{ae}\\ -\dfrac{\sqrt{Y_0}}{Y_0+Y}\mathbf{M}_{ea} & \dfrac{Y_0-Y}{Y_0+Y}\end{bmatrix} \tag{1.7}$$

or in the scalar form

$$\mathbf{S}=\begin{bmatrix}m_{11}-\dfrac{m_{13}m_{31}}{Y_0+Y} & m_{12}-\dfrac{m_{13}m_{32}}{Y_0+Y} & \dfrac{2\sqrt{Y_0}m_{13}}{Y_0+Y}\\ m_{21}-\dfrac{m_{23}m_{31}}{Y_0+Y} & m_{22}-\dfrac{m_{23}m_{32}}{Y_0+Y} & \dfrac{2\sqrt{Y_0}m_{23}}{Y_0+Y}\\ -\dfrac{\sqrt{Y_0}m_{31}}{Y_0+Y} & -\dfrac{\sqrt{Y_0}m_{32}}{Y_0+Y} & \dfrac{Y_0-m_{33}}{Y_0+Y}\end{bmatrix} \tag{1.8}$$

where $Y_0=1/Z_0$ is the characteristic admittance at the electric port and $Y=m_{33}$ is the transducer admittance.

For a reciprocal and lossless network, the wave scattering matrix is symmetric $\mathbf{S}=\mathbf{S}^{\mathrm{T}}$ and unitary $\mathbf{SS}^*=\mathbf{E}$ [3] where * denotes Hermitian conjugation of a matrix and **E** is the identity matrix. The reciprocity (symmetry) property of the wave scattering matrix **S** leads to the following reciprocity relations for the mixed scattering matrix blocks

$$\mathbf{M}_{aa}=\mathbf{M}_{aa}^{\mathbf{T}} \qquad (\textit{acoustic part}) \tag{1.9}$$

$$\mathbf{M}_{ea}=-2\mathbf{M}_{ae}^{\mathbf{T}} \qquad (\textit{acoustoelectric part}) \tag{1.10}$$

The unitary (power conservation) property of the wave scattering matrix **S** for a lossless SAW transducer imposes additional restrictions on its elements and hence the elements of the mixed scattering matrix **M**. In the block-matrix form this property can be written as

$$\mathbf{SS}^*=\begin{bmatrix}\mathbf{S}_{aa} & \mathbf{S}_{ae}\\ \mathbf{S}_{ea} & \mathbf{S}_{ee}\end{bmatrix}\begin{bmatrix}\mathbf{S}_{aa} & \mathbf{S}_{ae}\\ \mathbf{S}_{ea} & \mathbf{S}_{ee}\end{bmatrix}^*=\begin{bmatrix}\mathbf{S}_{aa}\mathbf{S}_{aa}^*+\mathbf{S}_{ae}\mathbf{S}_{ae}^* & \mathbf{S}_{aa}\mathbf{S}_{ea}^*+\mathbf{S}_{ae}\mathbf{S}_{ee}^*\\ \mathbf{S}_{ea}\mathbf{S}_{aa}^*+\mathbf{S}_{ee}\mathbf{S}_{ae}^* & \mathbf{S}_{ea}\mathbf{S}_{ea}^*+\mathbf{S}_{ee}\mathbf{S}_{ee}^*\end{bmatrix}=\begin{bmatrix}\mathbf{E} & \mathbf{0}\\ \mathbf{0}^{\mathbf{T}} & 1\end{bmatrix} \tag{1.11}$$

where $\mathbf{E}=\begin{bmatrix}1 & 0\\ 0 & 1\end{bmatrix}$ is the identity matrix of 2 by 2 size and $\mathbf{0}=[0\ \ 0]^{\mathbf{T}}$**.** The block-matrix equation (1.11) is reduced to the following system of equations

$$\begin{cases}\mathbf{S}_{aa}\mathbf{S}_{aa}^*+\mathbf{S}_{ae}\mathbf{S}_{ae}^*=\mathbf{E} & (1.12)\\ \mathbf{S}_{aa}\mathbf{S}_{ea}^*+\mathbf{S}_{ae}\mathbf{S}_{ee}^*=\mathbf{0} & (1.13)\\ \mathbf{S}_{ea}\mathbf{S}_{ea}^*+\mathbf{S}_{ee}\mathbf{S}_{ee}^*=1 & (1.14)\end{cases}$$

Substitution of the matrix-blocks from Eq. (1.7) into Eq. (1.14) results in the following expression for the electric port radiation conductance in terms of the electrical and mixed units terms

$$\mathrm{Re}\{m_{33}\} = \frac{1}{4}\mathbf{M}_{ea}\mathbf{M}_{ea}^{*} = \mathbf{M}_{ae}^{*}\mathbf{M}_{ae} \tag{1.15}$$

We can see from Eq. (1.15) that according to the energy conservation law the electrical input (delivered) power is equal to the total acoustic output power in a lossless three-port. The contribution of SAW radiation to the imaginary (reactive) part $B(\omega)$ of the admittance $Y(\omega)=G(\omega)+jB(\omega)$ is related to the real part $G(\omega)$ by the Hilbert transformation due to the causality principle for the electrical current and voltage [4, 5] and can be calculated as

$$B(\omega) = \frac{1}{\pi}\int_{-\infty}^{\infty}\frac{G(\omega')}{\omega-\omega'}d\omega' \tag{1.16}$$

By substituting Eq. (1.7) into Eq. (1.13) and using Eq. (1.15) we derive the following equation interrelating the acoustic (dimensionless) and the mixed units terms

$$\mathbf{M}_{ae} = \frac{1}{2}\mathbf{M}_{aa}\mathbf{M}_{ea}^{*} \tag{1.17}$$

Finally, substitution of Eq. (1.7) into Eq. (1.12) and use of Eqs. (1.15), (1.17) give after some manipulations an equation for the acoustic part of the mixed scattering matrix

$$\mathbf{M}_{aa}\mathbf{M}_{aa}^{*} = \mathbf{E} \tag{1.18}$$

It is worthy to note that Eq. (1.18) follows directly from the consideration of a short-circuit transducer (passive grating) as a lossless two-port.

For convenience, we summarize the results by rewriting Eqs. (1.9), (1.10) and (1.15), (1.17) in the following scalar form.

Reciprocity:

$$m_{12} = m_{21} \tag{1.19}$$
$$m_{31} = -2\, m_{13} \tag{1.20}$$
$$m_{32} = -2\, m_{23} \tag{1.21}$$

***Power conservation (lossless three-port)*:**

$$|m_{11}|^2 + |m_{12}|^2 = 1 \tag{1.22}$$
$$|m_{22}|^2 + |m_{21}|^2 = 1 \tag{1.23}$$
$$m_{11}\, m_{12}^{*} + m_{22}^{*}\, m_{21} = 0 \tag{1.24}$$
$$\mathrm{Re}\{m_{33}\} = |m_{13}|^2 + |m_{23}|^2 \tag{1.25}$$

***Acoustoelectric conversion*:**

$$m_{13} = -(\, m_{23}^{*} + m_{22}\, m_{23}) \,/\, m_{21}^{*} \tag{1.26}$$
$$m_{23} = -(\, m_{13}^{*} + m_{11}\, m_{13}) \,/\, m_{12}^{*} \tag{1.27}$$

As for a reciprocal three-port $m_{12}=m_{21}$, it follows from Eqs. (1.22), (1.23) that $|m_{11}|=|m_{22}|=\sqrt{1-|m_{12}|^2}$.

Without the loss of generality, we can also presume that $m_{11}=m_{22}$ that can be adjusted by a proper location of the phase reference plane. Supposed for the reflection coefficient m_{11} to be known, the transmission coefficient $m_{12}=|m_{12}|e^{j\theta_{12}}$ can be determined with the magnitude $|m_{12}|=\sqrt{1-|m_{11}|^2}$ and phase $\theta_{12}=\theta_{11}\pm\pi/2$ that follows from Eq. (1.24) where θ_{11} is phase of the reflection coefficient m_{11}. Therefore, the reflection and transmission coefficients m_{11} и m_{12} are in phase-quadrature.

Thus, in general case the mixed scattering matrix **M** contains three principal elements m_{11}, m_{13}, and m_{33}. The transmission coefficient m_{12} can be deduced from the reflection coefficient m_{11} as was discussed. Given the acoustoelectric conversion function m_{13} in the left direction and the scattering coefficients m_{11} and m_{12}, the acoustoelectric conversion function m_{23} in the right direction can be determined by using Eq. (1.27), with the electroacoustic conversion functions m_{31} and m_{32} found by reciprocity, Eqs. (1.20), (1.21). The electric port admittance $m_{33}=Y(\omega)=G(\omega)+jB(\omega)$ should be deduced from physical considerations or calculated numerically by applying Eq. (1.25) to determine the real part (radiation conductance) $G(\omega)$, with the imaginary (reactive) part $B(\omega)$ given by Hilbert transformation of the radiation conductance $G(\omega)$.

1.3. Mixed Transmission Matrix of a SAW Transducer

The mixed scattering matrix $\mathbf{M}=[m_{ik}]$ of a SAW transducer describes relationship of the reflected waves b_1, b_2 and the terminal current I with the incident waves a_1, a_2 and the transducer bus-bar voltage V as follows

$$\begin{cases} b_1 = m_{11}a_1 + m_{12}a_2 + m_{13}V \\ b_2 = m_{21}a_1 + m_{22}a_2 + m_{23}V \\ I = m_{31}a_1 + m_{32}a_2 + m_{33}V \end{cases}. \tag{1.28}$$

Eq. (1.28) may be treated as a system of linear equations with respect to any set of three independent variables, either acoustic or electric ones.

In many applications, the mixed transmission matrix $\mathbf{T}=[t_{ik}]$, $i,k=1,2,3$ can be useful that describes relationship of the acoustic waves a_1, b_1 at the left acoustic port and the terminal current I with the waves a_2, b_2 at the right acoustic port and the transducer bus-bar voltage V, i.e.

$$\begin{cases} a_1 = t_{11}a_2 + t_{12}b_2 + t_{13}V \\ b_1 = t_{21}a_2 + t_{22}b_2 + t_{23}V \\ I = t_{31}a_2 + t_{32}b_2 + t_{33}V \end{cases} \tag{1.29}$$

or in matrix form

$$\begin{bmatrix} a_1 \\ b_1 \\ I \end{bmatrix} = \begin{bmatrix} t_{11} & t_{12} & t_{13} \\ t_{21} & t_{22} & t_{23} \\ t_{31} & t_{32} & t_{33} \end{bmatrix} \begin{bmatrix} a_2 \\ b_2 \\ V \end{bmatrix}. \tag{1.30}$$

The mixed transmission matrix **T** given by Eq. (1.30) is convenient for cascading SAW elements.

The elements t_{ik} of the mixed transmission matrix **T** can be found from the solution of the system (1.28) with respect to the unknown variables a_1, b_1 and I in terms of the variables a_2, b_2 and V supposed to be known a priori. After some manipulations, we obtain

$$\mathbf{T}=\begin{bmatrix} \dfrac{1}{m_{21}} & -\dfrac{m_{22}}{m_{21}} & -\dfrac{m_{23}}{m_{21}} \\ \dfrac{m_{11}}{m_{21}} & m_{12}-\dfrac{m_{11}m_{22}}{m_{21}} & m_{13}-\dfrac{m_{11}m_{23}}{m_{21}} \\ \dfrac{m_{31}}{m_{21}} & m_{32}-\dfrac{m_{22}m_{31}}{m_{21}} & m_{33}-\dfrac{m_{31}m_{23}}{m_{21}} \end{bmatrix}. \tag{1.31}$$

On the other hand, from the solution of Eq. (1.29) with respect to the unknown variables b_1, b_2 and I we can express the elements m_{ik} of the mixed scattering matrix **M** in terms of the elements t_{ik} of the mixed transmission matrix **T**

$$\mathbf{M}=\begin{bmatrix} \dfrac{t_{21}}{t_{11}} & t_{22}-\dfrac{t_{12}t_{21}}{t_{11}} & t_{23}-\dfrac{t_{21}t_{13}}{t_{11}} \\ \dfrac{1}{t_{11}} & -\dfrac{t_{12}}{t_{11}} & -\dfrac{t_{13}}{t_{11}} \\ \dfrac{t_{31}}{t_{11}} & t_{32}-\dfrac{t_{12}t_{31}}{t_{11}} & t_{33}-\dfrac{t_{13}t_{31}}{t_{11}} \end{bmatrix} \tag{1.32}$$

By using Eqs. (1.31) and (1.32) we can convert the mixed scattering matrix **M** to the mixed transmission matrix **T** and vice versa.

1.4. Scattering and Transmission Matrices in the Quasi-Static Approximation

If the central frequency of a SAW transducer is far away from the synchronous frequency it may be presumed to a good accuracy that a short-circuit SAW transducer is reflectionless ($m_{11}= m_{22}=0$). This is a basic assumption of the quasi-static approximation [4, 5] that simplifies considerably analysis of SAW transducers.

In this case, the mixed scattering matrix of the uniform SAW transducer takes the simple form

$$\mathbf{M}=\begin{bmatrix} 0 & e^{-j\Phi} & m \\ e^{-\Phi} & 0 & -m^{*}e^{-j\Phi} \\ -2m & m^{*}e^{-j\Phi} & Y \end{bmatrix} \tag{1.33}$$

where $\Phi=N\varphi$ is transducer phase delay, $\varphi=\beta p$ is the phase lag per period p, $\beta=\omega/v$ is SAW wave number, v is effective SAW velocity under the transducer, m is acoustoelectric conversion function, Y is the transducer admittance to satisfy the condition $\mathrm{Re}\{Y\}=2|m|^2$. Therefore, in the quasi-static approximation the mixed scattering matrix of a SAW transducer is characterized by three independent parameters:

1) effective SAW velocity v;
2) acoustoelectric conversion (transfer) function m;
3) transducer admittance $Y=G+jB+j\omega C$ where C is the transducer static capacitance.

Taking into account Eqs. (1.31) and (1.33) the mixed transmission matrix **T** in the quasi-static approximation (m_{11}= m_{22}=0, m_{12}= m_{21}=$e^{-j\Phi}$) takes the form

$$\mathbf{T}=\begin{bmatrix} e^{j\Phi} & 0 & -m_{23}e^{j\Phi} \\ 0 & e^{-j\Phi} & m_{13} \\ m_{31}e^{j\Phi} & m_{32} & m_{33}-m_{31}m_{23}e^{j\Phi} \end{bmatrix}=\begin{bmatrix} e^{j\Phi} & 0 & m^{*} \\ 0 & e^{-j\Phi} & m \\ -2me^{j\Phi} & 2m^{*}e^{-j\Phi} & \mathrm{Im}\{m_{33}\} \end{bmatrix} \tag{1.34}$$

Eqs. (1.33) and (1.34) take the simplest form when the phase reference plane is chosen so that Φ=0, i.e. the phase is referenced to the transducer center. In this case, we obtain

$$\mathbf{M}=\begin{bmatrix} 0 & 1 & m \\ 1 & 0 & -m^{*} \\ -2m & 2m^{*} & Y \end{bmatrix} \tag{1.35}$$

and

$$\mathbf{T}=\begin{bmatrix} 1 & 0 & m^{*} \\ 0 & 1 & m \\ -2m & 2m^{*} & \mathrm{Im}\{Y\} \end{bmatrix}. \tag{1.36}$$

Therefore, only two independent matrix elements m and Y should be determined in the quasi-static approximation. In the next chapters we consider the calculation of the acoustoelectric conversion function m and the transducer admittance Y that includes the radiation conductance and susceptance as well as the static capacitance.

2. ACOUSTOELECTRIC CONVERSION FUNCTION

2.1. Definition of the Acoustoelectric Conversion Function

By definition, the acoustoelectric conversion (transfer) function is given by the following expression $m=a_1/V$ where a_1 is the generalized SAW amplitude of the wave traveling in the left direction, V is the voltage applied across the transducer. To deduce a closed-form equation for the acoustoelectric conversion function, we express a generalized SAW amplitude a in terms of the surface wave potential ϕ. In the quasi-static approximation, SAW power flow carried by the uniform acoustic beam of the width W (acoustic aperture) is given by [5, Eq. (3.34)]

$$P = \frac{1}{2} a a^* = \frac{1}{2} Y_0 \phi \phi^* = \frac{1}{4} \frac{\omega W}{\Gamma} \phi \phi^* \tag{2.1}$$

where the potential ϕ accompanies the traveling surface wave of the amplitude a, $\Gamma=K^2/2\varepsilon$ is the substrate material constant, K^2 is the piezoelectric coupling factor, $\varepsilon=\varepsilon_0+\varepsilon_p$ is the surface effective permittivity, ε_0 is the permittivity of the medium above the substrate surface, and ε_p is the permittivity of the substrate material. Therefore, a generalized SAW amplitude a is related with a SAW potential ϕ as

$$a = \sqrt{Y_0}\,\phi \tag{2.2}$$

where $Y_0=\omega W/2\Gamma$ is the acoustic characteristic admittance of the substrate material.

The potential ϕ of the surface acoustic wave launched by a periodic SAW transducer in the left direction is known to be [5, Eq. (4.87)]

$$\phi(\beta) = j\varepsilon\Gamma V \xi(\beta) F(\beta) e^{-j\beta L/2} \tag{2.3}$$

where $\beta=\omega/v$ is the SAW wave number, $\xi(\beta)$ is the element factor and $F(\beta)$ is the array factor, $L=Np$ is the transducer length, with N being the number of electrodes (fingers) and p being the finger pitch (period) (Fig. 2.1).

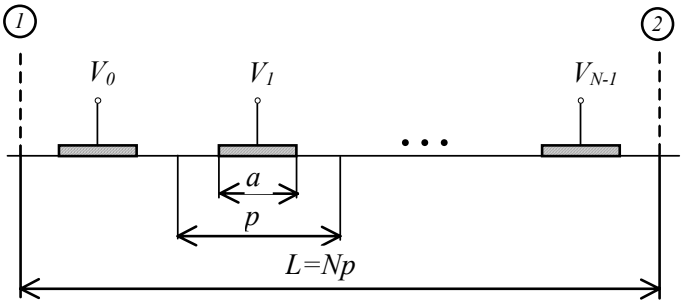

Fig. 2.1. Finite length periodic SAW transducer

The element factor is defined as [5-7]

$$\xi(\nu) = \frac{2\sin\pi\nu}{P_{-\nu}(-\cos\Delta)} P_n(\cos\Delta) \tag{2.4}$$

where $\nu=\varphi/2\pi-n$ is the baseband normalized frequency variable, $\varphi=\beta p$ is the phase lag per period p, β is the SAW wavenumber, $n=[\varphi/2\pi]$ is the space harmonic number ($n \le \varphi/2\pi \le n+1$), $P_{-\nu}(-\cos\Delta)$ is the Legendre function, $P_n(-\cos\Delta)$ is the Legendre polynomial, $\Delta=\pi\eta$, $\eta=a/p$ is the metallization ratio (duty factor), a is the finger width.

The array factor $F(\varphi)$ is given by the Fourier transform of the set of electrode potentials V_k, $k=0,N-1$ [5]:

$$F(\varphi) = \frac{1}{V}\sum_{k=0}^{N-1} V_k e^{-j(k-\frac{N-1}{2})\varphi} \tag{2.5}$$

where phase is referenced to the transducer center. Taking into account Eqs. (2.2)-(2.4) we obtain the following explicit formula for the acoustoelectric conversion function

$$m = a_1/V = \sqrt{Y_0}\phi/V = \frac{j}{2}\sqrt{\omega W K^2 \varepsilon}\,\xi(\varphi)F(\varphi)e^{-j\Phi/2} \tag{2.6}$$

where $\Phi=\beta L=N\beta p$.

Eq. (2.6) has been deduced in terms of finger taps which are specified by a set of the prescribed potentials V_k on the transducer electrodes. The correct modeling of periodic SAW transducers presumes introducing two semi-infinite additional sets of the equipotential guard electrodes to suppress the electrostatic end effects in the finite length transducer [5, 8]. These guard electrodes have the potentials $V_k=V_0$, $k<0$ and $V_k=V_{N-1}$, $k>N-1$ at the left and right sides of the basic structure with the potentials V_k, $k=0,N-1$ (Fig. 2.2).

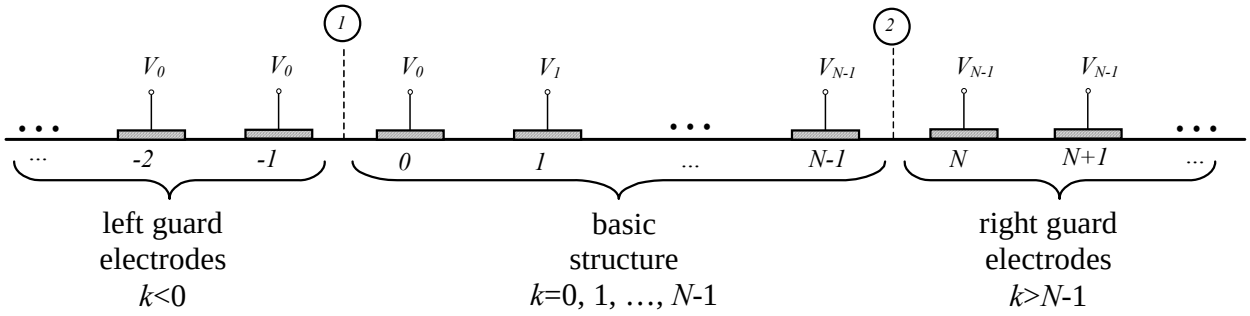

Fig. 2.2. Periodic SAW transducer with guard electrodes

In particular case of the grounded guard fingers ($V_0=V_{N-1}=0$), the summation involves only the basic structure with the finite number of fingers N. However, in general case $V_0 \neq V_{N-1} \neq 0$ the summation in Eq. (2.5) has to be extended to include contribution of the guard fingers. Without loss of generality, we place for the moment the phase reference in the center of the first finger of the basic structure. Then by using the identities

$$\sum_{k=0}^{N-1} e^{\pm jk\varphi} = \frac{1-e^{\pm jN\varphi}}{1-e^{\pm j\varphi}}$$

$$\sum_{k=0}^{\infty} e^{\pm jk\varphi} = \frac{1}{1-e^{\pm j\varphi}}$$

the sum in Eq. (2.5) can be modified as

$$\sum_{k=-\infty}^{\infty} V_k e^{-jk\varphi} = V_0 \sum_{k=-\infty}^{-1} e^{-jk\varphi} + \sum_{k=0}^{N-1} V_k e^{-jk\varphi} + V_{N-1} \sum_{k=N}^{\infty} e^{-jk\varphi} = \sum_{k=0}^{N-1} V_k e^{-jk\varphi} + \frac{V_{N-1} e^{-jN\varphi} - V_0}{1 - e^{-j\varphi}} \tag{2.7}$$

After simple transformations, we obtain

$$F(\varphi) = \frac{1}{V} \left\{ \sum_{k=0}^{N-1} (V_k - V_{N-1}) e^{-jk\varphi} + \frac{V_{N-1} - V_0}{1 - e^{-j\varphi}} \right\} \tag{2.8}$$

where the last term accounts for the contribution of the guard electrodes. We can see that only in the particular case V_0=V_{N-1}=0 Eq. (2.8) reduces to Eq. (2.5). It is worthy to note that according to Eq. (2.8) applying a uniform potential across all the fingers including guard ones doesn't affect the transducer response that is anticipated from the physical considerations.

After some manipulations, the sum (2.7) can be transformed to another form

$$\sum_{k=-\infty}^{\infty} V_k e^{-jk\varphi} = \frac{1}{1 - e^{-j\varphi}} \left(\sum_{k=1}^{N} V_k e^{-jk\varphi} - \sum_{k=0}^{N-1} V_k e^{-j(k+1)\varphi} \right) = \frac{1}{2j \sin\varphi/2} \sum_{k=0}^{N-1} \Delta V_k e^{-j(k+\frac{1}{2})\varphi} \tag{2.9}$$

where $\Delta V_k = V_{k+1} - V_k$ is the voltage in the *k*-th gap between the adjacent fingers having the potentials V_{k+1} and V_k, respectively. The factor $e^{-j(k+1/2)\varphi}$ accounts for the gap position offset with respect to the finger center. As the last gap voltage in Eq. (2.9) $\Delta V_{N-1} = V_N - V_{N-1}$=0, the summation corresponds to the number of the actual gaps *M=N-1* in the basic structure.

Eq. (2.9) shows that the array factor can be alternatively expressed in terms of the Fourier transform of the gap voltages ΔV_k. This form is more convenient for practical use as it gives zero contribution of the guard fingers to the overall response regardless a set of potentials V_k. Since we use the voltages ΔV_k instead of the potentials V_k, this excludes automatically any uniform potential applied across the transducer.

Referenced to the transducer center, Eq. (2.9) gives the following equation for the array factor

$$F(\varphi) = \frac{1}{2j \sin\varphi/2} \frac{1}{V} \sum_{k=0}^{M-1} \Delta V_k e^{-j(k - \frac{M-1}{2})\varphi} \tag{2.10}$$

where *M=N-1* is the number of gaps in the basic structure. After substitution of Eq. (2.10) into Eq. (2.6), we obtain the expression for the acoustoelectric conversion function in terms of the gap voltages

$$m = \frac{1}{2} \sqrt{\omega W K^2 \varepsilon}\, \zeta(\varphi) \Delta F(\varphi) e^{-j\beta L/2} \tag{2.11}$$

where the gap element factor $\zeta(\varphi)$ is related to the finger element factor $\xi(\varphi)$ as

$$\zeta(\varphi) = \xi(\varphi) / 2\sin\varphi/2 = \frac{P_n(\cos\Delta)}{P_{-\nu}(-\cos\Delta)}, \qquad \nu = \varphi/2\pi. \tag{2.12}$$

and the gap array factor

$$\Delta F(\varphi) = \frac{1}{V} \sum_{k=0}^{M-1} \Delta V_k e^{-j(k - \frac{M-1}{2})\varphi} \tag{2.13}$$

According to Eq. (2.12) the gap element factor has the simpler form and weaker frequency dependence if compared to the finger element factor that is an additional advantage of using gap voltages instead of the finger potentials.

2.2. Acoustoelectric Conversion Function for Apodized SAW Transducer

For an apodized periodic SAW transducer, the acoustic field variables in equations vary with the coordinate *y* across the acoustic aperture *W*, as well as with *x* in the propagation direction. We confine our consideration to cases where the propagating wavefront is intercepted by a uniform receiving SAW transducer or by a multistrip coupler. In these cases, the detected signal is not affected if the actual two-dimensional distribution $\phi(x,y)$ of the surface wave potential is replaced by the averaged distribution $\overline{\phi}(x)$ over the acoustic aperture *W* [8] with the Fourier transform

$$\overline{\phi}(\beta) = \frac{1}{W}\int_{-W/2}^{W/2} \phi(\beta, y)dy = j\varepsilon V \xi(\beta)\overline{F}(\beta)e^{-j\beta L/2} \tag{2.14}$$

where in terms of the finger taps the averaged array factor

$$\overline{F}(\varphi) = \frac{1}{W}\int_{-W/2}^{W/2} F(\varphi, y)dy = \frac{1}{V}\sum_{k=0}^{N-1}\overline{V}_k e^{-j(k-\frac{N-1}{2})\varphi} \tag{2.15}$$

To determine the averaged potentials $\overline{V}_k$ across the aperture *W*, we consider an array with two parallel bus-bars supplied with the potentials $\pm\Delta V/2$ and with the set of fingers with potentials $V_k=\pm\Delta V/2$. Each electrode is connected to either of the bus-bars and is complemented by a dummy finger for the wave front equalization (Fig. 2.3).

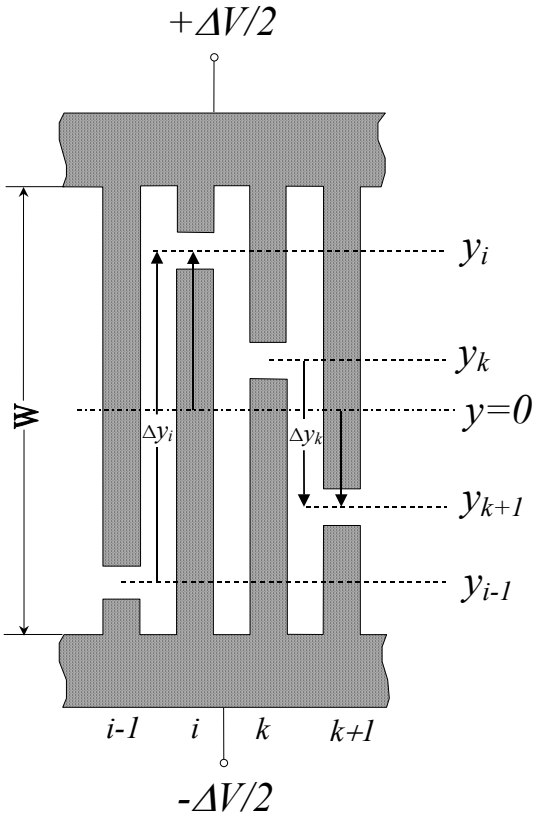

Fig. 2.3. Finger and gap tap weights of the apodized SAW transducer

The transducer apodization pattern is specified by the positions y_k of the transversal gaps defined as the

finger length from the center line $y=0$ in the middle of the aperture. The transversal gaps are the gaps separating active fingers and dummy fingers of the opposite polarity (Fig. 2.3). The mean potential $\overline{V}_k$ averaged across the aperture W can be found as

$$\overline{V}_k = \frac{1}{W}\int_{-W/2}^{W/2} V_k(y)dy = \frac{1}{W}\int_{-W/2}^{y_k} V_k(y)dy + \frac{1}{W}\int_{y_k}^{W/2} V_k(y)dy = \frac{\Delta V}{2}(\frac{1}{2} - y_k/W) - \frac{\Delta V}{2}(\frac{1}{2} + y_k/W) = -\frac{y_k}{W}\Delta V \tag{2.16}$$

where ΔV is the voltage applied to the transducer bus-bars.

Correspondingly, the mean gap voltage $\Delta\overline{V}_k = \overline{V}_{k+1} - \overline{V}_k$ is given by

$$\Delta\overline{V}_k = -\frac{\Delta y_k}{W}\Delta V \tag{2.17}$$

where $\Delta y_k = y_{k+1} - y_k$ is the overlap of the adjacent fingers with transversal gap positions y_{k+1} and y_k, respectively. Thus, the effective finger and gap tap weights $\overline{V}_k$ and $\Delta\overline{V}_k$ are essentially fractions of the bus-bar voltage ΔV which are proportional to the normalized transversal gap coordinate y_k/W and fractional overlap $\Delta y_k/W$, respectively. For calculation of the acoustoelectric conversion function of the apodized periodic SAW transducer, the effective tap weights (2.16) and (2.17) should be substituted into Eqs. (2.5), (2.6) and (2.10), (2.11) instead of the conventional potentials V_k or gap voltages ΔV_k.

3. ADMITTANCE CALCULATION FOR PERIODIC SAW TRANSDUCERS

3.1. Introduction

SAW transducer admittance calculation is an integral part of the computer-aided design of SAW bandpass filters. Accurate modeling is necessary to predict a priori SAW filter insertion loss, simulate frequency response distortion due to the electrical interaction with source and load, match perfectly SAW devices. Unfortunately, rigorous analysis techniques [9] are impracticable due to the intrinsic complexity and computational slowness. In practice, the equivalent circuit model of the uniform SAW transducer is used [10] and aperture-channelizing technique [11, 12] is applied to model apodized SAW transducers. It is the transducer radiation conductance that is first calculated within SAW transducer model and then the numerical Hilbert transformation is performed to calculate the radiation susceptance [11].

Calculations are simplified in the quasi-static approximation [5] where superposition principle can be effectively applied to calculate radiation conductance of an unapodized periodic SAW transducer with an arbitrary polarity sequence [11, 12]. Unfortunately, simple analytic formulae comprising both radiation conductance and susceptance were deduced for uniform multielectrode transducers only [13].

A comprehensive approach to the analysis problem for periodic SAW transducers in the quasi-static approximation has been developed and implemented by the author in [14-16]. The closed-form equations for admittance calculation comprising both acoustic conductance and susceptance have been deduced using the concept of the nodal admittance matrix of a SAW transducer [15]. It will be shown that within the model constraints applied the acoustic admittance of an aperture-weighted (apodized) SAW transducer can be treated as a weighted sum of the elemental interelectrode admittances, with the weights given by the overlaps (partial apertures) of the fingers. The nodal admittance matrix takes the simplest form for periodic SAW transducers with a fixed pitch and metallization ratio. In this case, the general formula for apodized periodic SAW transducers may be converted to the compact form by applying a special summation technique and taking into account the periodic properties of the nodal matrix [15].

3.2. Nodal Admittance Matrix of a SAW Transducer

We shall deduce the closed-form equation for admittance calculation comprising both acoustic conductance and susceptance using a concept of the nodal admittance matrix of a SAW transducer in the quasi-static approximation. The nodal admittance matrix takes the simplest form for periodic SAW transducers with a fixed pitch (period) and metallization ratio.

It can be shown using superposition principle that electrode currents I_i and voltages V_k are interrelated via the nodal admittance matrix with the elements Y_{ik} as follows

$$\mathbf{I} = \mathbf{YV} \tag{3.1}$$

where $\mathbf{I}=[I_0\ I_1\ \dots\ I_{N-1}]$ is vector of the electrode currents, $\mathbf{V}=[V_0\ V_1\ \dots\ V_{N-1}]$ is vector of the electrode potentials, and $\mathbf{Y}=[Y_{ik}]$, $i,k=0,N-1$ is the square nodal admittance matrix of the size N, with N being the electrode number of a SAW transducer. Due to the reciprocity property, the nodal admittance matrix is symmetrical $Y_{ik}=Y_{ki}$ and due to the causality principle for the voltages and currents, the real and imaginary parts of each element $Y_{ik}=G_{ik}+jB_{ik}$ are interrelated via a Hilbert transformation (1.16).

The elements Y_{ik} of the nodal admittance matrix are defined as

$$Y_{ik}(\omega) = I_i(\omega)/V_k, \quad V_i = 0, i \neq k \tag{3.2}$$

where $I_i(\omega)$ is the current induced in the i-th electrode when the k-th electrode is activated by applying the voltage V_k, with all the others being grounded (Fig. 3.1).

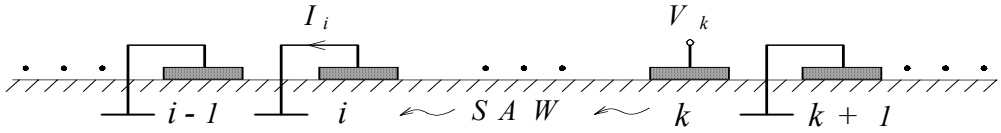

Fig. 3.1. Acoustoelectric interaction of the i-th and k-th electrodes in the elemental SAW transducer

In general case, the currents $I_i(\omega)$ contain both the acoustic and electrostatic components. The electrostatic component $j\omega Q_i$ with Q_i being the electrostatic charge on the i-th electrode can be found from the solution of the electrostatic problem and contributes to the transducer static capacitance. In this chapter, our primary concern is focused on the calculation of the acoustic component of the current $I_i(\omega)$ that is induced by the incident acoustic wave generated by the k-th electrode, with the electrostatic component omitted. A closed-form charge and capacitance calculation for the case of periodic SAW transducers will be discussed in Chapter 4.

In the quasi-static approximation, the short-circuit current $I_i(\omega)$ induced acoustically in the i-th electrode of the aperture W by the k-th electrode with the applied voltage V_k can be written in the form [4, 5]

$$I_i(\omega) = \omega W \Gamma V_k \begin{cases} \rho_i^*(\omega)\rho_k(\omega)e^{-j\beta l_{ik}}, & i < k \\ \rho_i(\omega)\rho_k^*(\omega)e^{-j\beta l_{ik}}, & i \geq k \end{cases} \tag{3.3}$$

where $\Gamma = K^2/2\varepsilon$ is the piezoelectric constant of a substrate material, with K^2 being the electromechanical coupling factor and ε being the substrate effective permittivity, $\beta = \omega/v$ is the SAW wavenumber, v is the SAW velocity, l_{ik} is the separation between i-th and k-th electrodes. The function $\rho_k(\omega)$ is the Fourier transform of the electrostatic charge density distribution [5] in the elemental SAW transducer structure where the potential V_k is applied to the k-th electrode, with all the others grounded.

For periodic SAW transducers with a fixed pitch (period) p and a constant metallization ratio $\eta = a/p$ where a is the finger width, it follows [5] that $\rho_i^*(\omega) = \rho_k(\omega) = \rho(\omega) = \varepsilon\xi(\omega)$ where the function $\xi(\omega)$ is given by Eq. (2.4). Then the elements $Y_{ik}(\omega)$ of the nodal admittance matrix defined per unit aperture are given by the following equation [14, 15]

$$Y_{ik}(\omega) = 0.5\omega K^2 \varepsilon \xi^2(\omega) \begin{cases} e^{-j|i-k|\varphi}, & i \neq k \\ (1 + j\,\mathrm{ctg}\,\varphi/2), & i = k \end{cases} \tag{3.4}$$

where $\varphi = \beta p$ is the phase lag per period, $\beta = \omega/v$ is the SAW wavenumber. In Eq. (3.4) the electrode self-admittance with an additional term $j\mathrm{ctg}\varphi/2$ can be deduced by applying Eq. (3.3) in the particular case $i = k$ that gives the radiation conductance, with the radiation susceptance found by the closed-form Hilbert transformation (1.16) of the self-admittance radiation conductance to satisfy the causality

principle [14].

The nodal admittance matrix with the elements (3.4) has some useful properties. According to Eq. (3.4), the matrix elements depend on the indexes difference, i.e. $Y_{ik}(\omega)=Y_{|i-k|}(\omega)$ that allows to introduce one-dimension indexing of the matrix elements $p=|i-k|$. Therefore, the overall nodal admittance matrix **Y** contains N different elements $Y_{|i-k|}(\omega)$ only, with each sequential row (column) derived by the cyclic shift of the preceding one.

According to the physical meaning of the nodal admittances $Y_{ik}(\omega)$ in the electrical circuit theory, the elements $Y_p(\omega)=-Y_{|i-k|}(\omega)$, $p>0$ may be treated as the mutual (interelectrode) partial admittances connected to the nearest fingers, next nearest ones, etc. (Fig. 3.2).

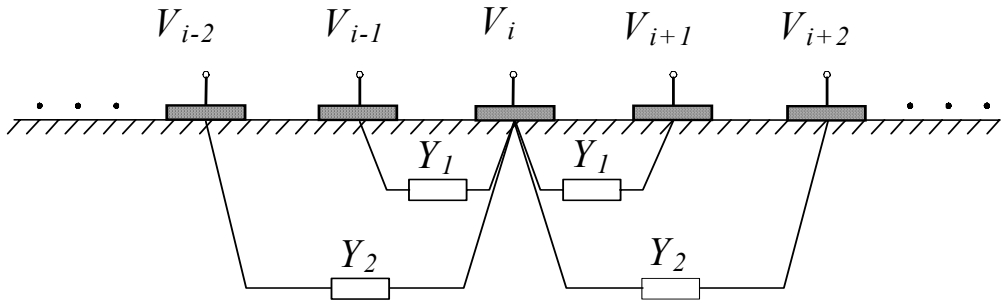

Fig. 3.2. Mutual partial admittances connected to the *i*-th electrode

Thus, the nodal admittance matrix **Y** has the following structure

$$\mathbf{Y} = -\begin{bmatrix} Y_0(\omega) & Y_1(\omega) & Y_2(\omega) & \dots & Y_{N-1}(\omega) \\ Y_1(\omega) & Y_0(\omega) & Y_1(\omega) & \dots & Y_{N-2}(\omega) \\ \vdots & & \ddots & & \vdots \\ Y_{N-2}(\omega) & Y_{N-3}(\omega) & \dots & Y_0(\omega) & Y_1(\omega) \\ Y_{N-1}(\omega) & Y_{N-2}(\omega) & \dots & Y_1(\omega) & Y_0(\omega) \end{bmatrix} \tag{3.5}$$

where for convenience we define $Y_0(\omega)=-Y_{00}(\omega)$ as the self-admittance.

As a consequence of the Kirchhoff's law we can also predict

$$\sum_{i=-\infty}^{\infty} Y_{ik} = \sum_{k=-\infty}^{\infty} Y_{ik} = Y_{00} + 2\sum_{p=1}^{\infty} Y_{i,i+p} = Y_0(\omega) + 2\sum_{p=1}^{\infty} Y_p(\omega) = 0 \tag{3.6}$$

where summation is taken within infinite limits to account for correctly all the electrode currents in the theoretically infinite periodic structure [5]. The identity (3.6) can be verified by direct substitution of Eq. (3.4) into (3.6). On the other hand, the formula (3.6) obtained from the physical considerations gives also the way for deducing the correct equation for the self-admittance $Y_0(\omega)$ from the knowledge of the mutual admittances $Y_p(\omega)$ as

$$Y_0 = -2\sum_{p=1}^{\infty} Y_p = \omega K^2 \varepsilon\xi^2(\omega) \sum_{p=1}^{\infty} e^{-jp\varphi} = \omega K^2 \varepsilon\xi^2(\omega) \frac{e^{-1}}{1-e^{-1}} = -0.5\,\omega K^2 \varepsilon\xi^2(\omega)(1 + j\,\mathrm{ctg}\,\varphi/2) \tag{3.7}$$

that excludes the closed-form Hilbert transformation of the self-admittance to satisfy the causality principle.

If the number of electrodes N is large enough we can assume with a sufficient accuracy that

$$Y_0 \approx -2\sum_{p=1}^{N-1} Y_p \tag{3.8}$$

Thus, the nodal admittance matrix for the periodic SAW transducer is completely defined, with all its elements correctly determined.

3.3. Admittance of an Unapodized SAW Transducer

3.3.1. Calculation in Terms of Finger Potentials

Given the nodal admittance matrix **Y** and the set of the SAW transducer electrode potentials **V**, we can deduce a closed-form equation for the transducer admittance from the following energy conservation considerations. In the quasi-static approximation, the total (radiated and stored) acoustic power flow in a SAW transducer of the unit aperture W=1 is given by the following equation

$$P = \frac{1}{2}\mathbf{V}^*\mathbf{I} = \frac{1}{2}Y(\omega)\Delta V^2 \tag{3.9}$$

where $Y(\omega)$ is the transducer acoustic admittance, ΔV is the voltage applied to the transducer bus-bars, **V** and **I** are vectors of the electrode voltages and currents, respectively, and the asterisk denotes Hermitian conjugation. By taking into account Eq. (3.1) we can derive the following matrix equation for transducer admittance

$$Y(\omega) = \frac{1}{\Delta V^2}\mathbf{V}^*\mathbf{I} = \frac{1}{\Delta V^2}\mathbf{V}^*\mathbf{Y}\mathbf{V} \tag{3.10}$$

or in scalar form

$$Y(\omega) = \frac{1}{\Delta V^2}\sum_{i=0}^{N-1}\sum_{k=0}^{N-1} Y_{ik}(\omega)V_iV_k = \frac{1}{2}\sum_{i=0}^{N-1}\sum_{k=0}^{N-1}(1+\delta_{ik})W_{ik}Y_{ik}(\omega) = \sum_{i=0}^{N-1}\sum_{k=0}^{N-1-i} W_{ik}Y_{ik}(\omega) \tag{3.11}$$

where $W_{ik} = \dfrac{2}{1+\delta_{ik}}\dfrac{V_iV_k}{\Delta V^2} = \begin{cases} 2V_iV_k/\Delta V^2, & i \neq k \\ V_i^2/\Delta V^2, & i = k \end{cases}$, $\delta_{ik} = \begin{cases} 1, & i = k \\ 0, & i \neq k \end{cases}$.

The last form of Eq. (3.11) accounts for that each mutual nodal admittance $Y_{ik}(\omega)$, $i \neq k$ is included in the double summation twice. We can also rewrite Eq. (3.11) using the concept of partial admittances $Y_p(\omega)$ as follows

$$Y(\omega) = -\sum_{p=0}^{N-1}\sum_{i=0}^{N-1-p} W_{i,i+p}Y_p(\omega) = -\sum_{p=0}^{N-1}\sum_{i=p}^{N-1} W_{i,i-p}Y_p(\omega) \tag{3.12}$$

According to Eq. (3.12) the transducer admittance is the weighted sum of the partial admittances $Y_p(\omega)$. If each electrode is connected to either of two bus-bars having the potentials $\pm\Delta V/2$ then the weights W_{ik} take the value +1/2 for all the electrode pairs with the same potentials V_i=V_k and the value –1/2 otherwise. If one of the bus-bar has the applied potential ΔV (“hot” bus-bar) and another is grounded (zero potential), the weights W_{ik} take the values 2 and 0, respectively.

By using the identity $-2V_i V_k=(V_i-V_k)^2 - V_i^2 - V_k^2$ and omitting the terms which depend on one index

only as giving negligible contribution for large N due to the property (3.8), we obtain

$$Y(\omega) \approx \frac{1}{\Delta V^2} \sum_{p=0}^{N-1} \sum_{i=0}^{N-1-p} \Delta V_{i,i+p}^2 Y_p(\omega) = \frac{1}{\Delta V^2} \sum_{p=0}^{N-1} \sum_{i=p}^{N-1} \Delta V_{i,i-p}^2 Y_p(\omega) \tag{3.13}$$

where $\Delta V_{i,i\pm p} = \left| V_i - V_{i\pm p} \right| = \begin{cases} \Delta V, & V_i \neq V_{i\pm p} \\ 0, & V_i = V_{i\pm p} \end{cases}$.

Eq. (3.13) has a clear physical meaning that the essential contribution to the admittance is given by the electrode pairs of the opposite polarities.

After substituting Eq. (3.4) into (3.11) and using the identity

$$\left| \sum_{k=0}^{N-1} V_k e^{-jk\varphi} \right|^2 = \left(\sum_{i=0}^{N-1} V_i \quad e^{-ji\varphi} \right) \left(\sum_{k=0}^{N-1} V_k e^{-jk\varphi} \right)^* = \sum_{i=0}^{N-1} \sum_{k=0}^{N-1} V_i V_k \cos(i-k)\varphi = \mathrm{Re} \left\{ \sum_{i=0}^{N-1} \sum_{k=0}^{N-1} V_i V_k e^{|i-k|\varphi} \right\} \tag{3.14}$$

we deduce from the real part of Eq. (3.11) the known expression for the acoustic conductance [5, Eq. 4.105]

$$G(\omega) = \frac{1}{\Delta V^2} \omega W \Gamma \rho^2(\omega) \left| \sum_{k=0}^{N-1} V_k e^{-j k \varphi} \right|^2 \tag{3.15}$$

where $\rho(\omega)=\varepsilon\xi(\omega)$. Contrary to Eq. (3.15) which is valid for the radiation conductance of the unapodized SAW transducers only, Eq. (3.11) is much more general as it allows to calculate simultaneously the conductance $G(\omega)$ and susceptance $B(\omega)$ of the transducer admittance $Y(\omega)=G(\omega)+jB(\omega)$. As will be shown later, Eq. (3.11) is also valid for apodized SAW transducers, with the weights W_{ik} properly defined.

3.3.2. Calculation in Terms of Gap Voltages

In general case, the correct use of Eq. (3.11) should include summation in the infinite limits to account for contribution of the guard fingers. However, we can derive an accurate equation for admittance calculation in terms of gap voltages $\Delta V_k=V_{k+1}-V_k$ which comprises summation within basic structure only.

Given the vector of the gap voltages $\mathbf{\Delta V}=[\Delta V_0\ \Delta V_1 \ldots \Delta V_{N-1}]^T$, the vector of the finger potentials $\mathbf{V}=[V_0\ V_1 \ldots V_{N-1}]^T$ can be found as

$$\mathbf{V} = -\mathbf{U}\Delta\mathbf{V} + \mathrm{const} \tag{3.16}$$

or in scalar form

$$V_i = -\sum_{k=0}^{N-1} U_{ik} \Delta V_k = -\sum_{k=i}^{N-1} \Delta V_k + \mathrm{const} \tag{3.17}$$

where the upper-triangular matrix $\mathbf{U}=[U_{ik}]$ contains units in the upper (non-zero) part and zeros in the lower part

$$\mathbf{U}=\begin{bmatrix}1 & 1 & 1 & \dots & 1\\ 0 & 1 & 1 & \dots & 1\\ 0 & 0 & 1 & \dots & 1\\ \vdots & & & \ddots & \vdots\\ 0 & 0 & 0 & \dots & 1\end{bmatrix} \tag{3.18}$$

By substituting Eq. (3.16) into (3.10) and extending the summation to the infinite limits corresponding to a transducer with guard fingers we obtain

$$Y(\omega)=\frac{1}{\Delta V^2}\Delta\mathbf{V}\,\hat{\mathbf{Y}}\,\Delta\mathbf{V} \tag{3.19}$$

or in scalar form

$$Y(\omega)=\frac{1}{\Delta V^2}\sum_{i=0}^{N-1}\sum_{k=0}^{N-1}\hat{Y}_{ik}\Delta V_i\Delta V_k \tag{3.20}$$

where the gap nodal admittance matrix is

$$\hat{\mathbf{Y}}=\mathbf{U}^{*}\mathbf{Y}\,\mathbf{U}=\mathbf{L}\mathbf{Y}\mathbf{U} \tag{3.21}$$

with the matrix $\mathbf{L}=\mathbf{U}^{*}=\mathbf{U}^{\mathrm{T}}$ being the lower-triangular unit matrix

$$\mathbf{L}=\begin{bmatrix}1 & 0 & 0 & \dots & 0\\ 1 & 1 & 0 & \dots & 0\\ 1 & 1 & 1 & \dots & 0\\ \vdots & & & \ddots & \vdots\\ 1 & 1 & 1 & \dots & 1\end{bmatrix}. \tag{3.22}$$

Eq. (3.21) may be rewritten in the following scalar form

$$\hat{Y}_{ik}=\sum_{m\le i}\sum_{n\le k}L_{im}Y_{mn}U_{nk}=\sum_{m\le i}\sum_{n\le k}Y_{mn}=\begin{cases}-\sum_{m>i}\sum_{n\le k}Y_{mn}, & i\ge k\\ -\sum_{m\le i}\sum_{n>k}Y_{mn}, & i\le k\end{cases} \tag{3.23}$$

where the property (3.6) has been applied to deduce the last identity. Using Eq. (3.21) and Eq. (3.4) we obtain the following relationship of the voltage (gap) and potential (finger) nodal admittances

$$\hat{Y}_{ik}=\hat{Y}_{ki}=-\sum_{m>i}\sum_{n\le k}Y_{mn}=-\sum_{p=0}^{\infty}\sum_{q=0}^{\infty}Y_{i+p+1,k-q}=\frac{1}{(1-e^{j\varphi})(1-e^{-j\varphi})}\begin{cases}Y_{ik}, & i\ne k\\ \mathrm{Re}\{Y_{ik}\}, & i=k\end{cases} \tag{3.24}$$

or

$$\hat{Y}_{ik}=\frac{1}{4\sin^2\varphi/2}\begin{cases}Y_{ik}, & i\ne k\\ \mathrm{Re}\{Y_{ik}\}, & i=k\end{cases}=0.5\,\omega WK^2\varepsilon\zeta^2(\varphi)\,e^{-j|i-k|\varphi} \tag{3.25}$$

where $\zeta(\varphi)=\xi(\varphi)/2\sin\varphi/2$ is the gap element factor given by Eq. (2.12).

The same result may be obtained by using Eq. (3.15) for the radiation conductance $G(\omega)$ in terms of the gap voltages instead of the finger potentials and applying the closed-form Hilbert transformation for calculation of the radiation susceptance $B(\omega)$.

Again, it is worthy noting that contrary to the finger taps using the gap taps assumes the finite summation over the basic structure as the gap voltages are identically equal to zero at the equipotential guard fingers.

3.4. Admittance of an Apodized SAW Transducer

3.4.1. Calculation in Terms of Finger Taps

We consider a periodic apodized IDT specified by the transversal gap positions y_k, k=0,N-1. In this case, all the acoustic and electric variables depend on the y-coordinate as well. However, Eq. (3.11) is applicable to a good accuracy to the elemental horizontal stripe of the width dy at an arbitrary intersection y (Fig. 3.3).

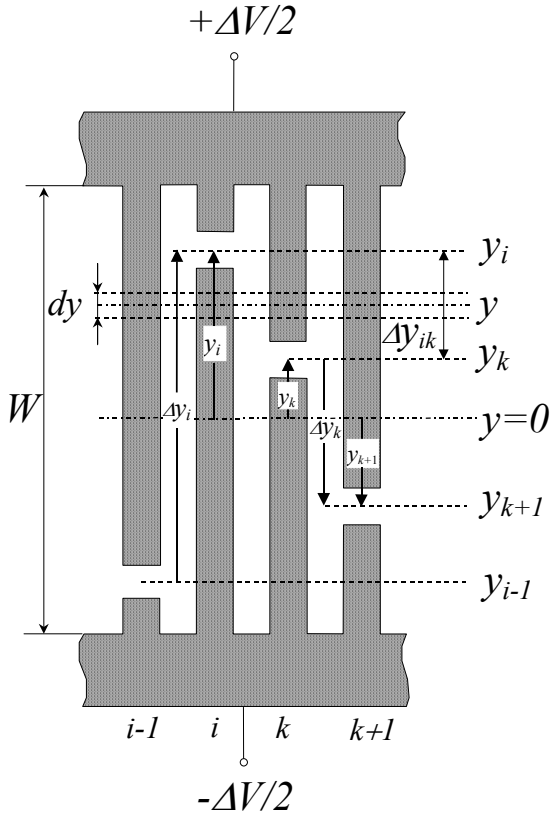

Fig. 3.3. Elemental intersection and taps of an apodized SAW transducer and partial apertures of the fingers and overlaps

The elemental stripe of width dy gives contribution $Y(\omega,y)dy$ to the total transducer admittance, with the admittance $Y(\omega,y)$ given by

$$Y(\omega, y) = \frac{1}{\Delta V^2} \sum_{i=0}^{N-1} \sum_{k=0}^{N-1} Y_{ik}(\omega) V_i(y) V_k(y) \tag{3.26}$$

where $V_i(y)$ is the potential on the i-th electrode at the intersection y. The total admittance $Y(\omega)$ of the apodized SAW transducer can be found by integrating Eq. (3.26) over the aperture W

$$Y(\omega) = \int_{-W/2}^{W/2} Y(\omega, y)dy = \sum_{i=0}^{N-1} \sum_{k=0}^{N-1-i} W_{ik} Y_{ik}(\omega) \tag{3.27}$$

where the weights

$$W_{ik} = \frac{1}{\Delta V^2} \int_{-W/2}^{W/2} \frac{2}{1+\delta_{ik}} V_i(y) V_k(y) dy = \begin{cases} \dfrac{W}{4}, & i = k \\ \dfrac{W}{2} - \Delta y_{ik}, & i \neq k \end{cases} \tag{3.28}$$

with the quantities $\Delta y_{ik} = |y_i - y_k|$ being overlaps (partial apertures) of the i-th and k-th electrodes with the coordinates of the transversal gaps y_i and y_k, respectively (Fig. 3.3).

For sufficiently long SAW transducers, we can neglect by the contribution of the constant term in (3.28) due to the property (3.6). Therefore, we obtain the following equation in terms of the partial admittances

$$Y(\omega) \approx \sum_{p=0}^{N-1} \sum_{i=0}^{N-1-p} \Delta y_{i,i+p} Y_p(\omega) = \sum_{p=0}^{N-1} \sum_{i=p}^{N-1} \Delta y_{i,i-p} Y_p(\omega) \tag{3.29}$$

Thus, the admittance of the apodized SAW transducer is the weighted sum of the elemental nodal admittances, with the weights given by the partial apertures Δy_{ik}. Eq. (3.29) can be reduced to the following compact form that minimizes considerably the computation time

$$Y(\omega) = \sum_{p=0}^{N-1} L_p Y_p(\omega) \tag{3.30}$$

where

$$L_p = \sum_{k=0}^{N-p-1} \Delta y_{k,\,k+p} \quad \text{or} \quad L_p = \sum_{k=p}^{N-1} \Delta y_{k,k-p} \ . \tag{3.31}$$

The quantities L_p are effective apertures composed of the total overlaps of all the nearest neighbor electrodes, next nearest ones, and so on, respectively. As can be seen from Eq. (3.31), the effective apertures depend on the SAW transducer apodization and do not depend on the frequency. Therefore, their computation is a single-time routine procedure, for a particular apodized SAW transducer. As the partial admittances $Y_p \sim e^{-jp\varphi}$ are proportional to the exponential function (see Eq. (3.4)), the transducer admittance $Y(\omega)=G(\omega)+jB(\omega)$ (3.30) is virtually defined by the Fourier transform of a set of the effective apertures L_p. Therefore, once a set of the effective apertures L_p has been calculated and stored in the memory, the calculation of SAW transducer admittance comprising both conductance $G(\omega)$ and susceptance $B(\omega)$ using Eq. (3.30) takes no more time than calculation of the transducer frequency response using Eqs. (2.13), (2.14). The Fast Fourier Transform (FFT) can be applied to admittance calculation in the wide frequency range to further reduce the computation time if necessary.

3.4.2. Calculation in Terms of Overlap Taps

By applying Eq. (3.20) to the elemental intersection of an apodized SAW transducer in the form

$$Y(\omega,y)=\frac{1}{\Delta V^2}\sum_{i=0}^{N-1}\sum_{k=0}^{N-1}\hat{Y}_{ik}(\omega)\Delta V_i(y)\Delta V_k(y)=\frac{1}{\Delta V^2}\sum_{i=0}^{N-1}\sum_{k=0}^{N-1}\hat{Y}_{ik}(\omega)\big(V_{i+1}(y)-V_i(y)\big)\big(V_{k+1}(y)-V_k(y)\big)=$$
$$\frac{1}{\Delta V^2}\sum_{i=0}^{N-1}\sum_{k=0}^{N-1}\hat{Y}_{ik}(\omega)\big[V_{i+1}(y)V_{k+1}(y)+V_i(y)V_k(y)-V_i(y)V_{k+1}(y)-V_{i+1}(y)V_k(y)\big] \quad (3.32)$$

we can deduce the following equation for the admittance $Y(\omega)$ of the apodized SAW transducer by integrating Eq. (3.32) over the aperture

$$Y(\omega)=\sum_{i=0}^{N-1}\sum_{k=0}^{N-1-i}\hat{W}_{ik}\hat{Y}_{ik}(\omega), \quad (3.33)$$

$$\hat{W}_{ik}=\frac{1}{\Delta V^2}\int_{-W/2}^{W/2}\frac{2}{1+\delta_{ik}}\Delta V_i(y)\Delta V_k(y)dy=\Delta y_{i+1,k}+\Delta y_{i,k+1}-\Delta y_{ik}-\Delta y_{i+1,k+1} \quad (3.34)$$

where the quantities $\Delta y_{ik}=|y_i-y_k|$ are overlaps of the i-th and k-th fingers. As integration in Eq. (3.34) gives non-zero contribution to $\hat{W}_{ik}$ only for those overlap regions where $\Delta V_i(y)\Delta V_k(y)\neq 0$, the physical meaning of the quantities $\hat{W}_{ik}$ is rather straightforward: this is the partial overlap of the i-th and k-th overlaps $\Delta y_i=y_{i+1}-y_i$ and $\Delta y_k=y_{k+1}-y_k$, respectively (Fig. 3.3). It follows that $0\le\hat{W}_{ik}\le\min\{|\Delta y_i|,|\Delta y_k|\}$, in general case.

3.5. Calculation Example and Experimental Results

An example of the modeled and measured admittance characteristics for a SAW bandpass filter is shown in Fig. 3.4. The SAW filter has the following parameters: central frequency f_0=42.7 MHz, fractional passband width (at -3 dB) 10 %, and shape factor of 2 (at -3 and -40 dB). The filter contains a regular unapodized and another apodized SAW transducer, both with split fingers (synchronous frequency $f_\pi=2f_0$). Electrode numbers are N_1=38 and N_2=118, respectively. The transducers have equal apertures W=2.35 mm and metallization ratio η=0.5. The substrate material is YZ lithium niobate with the electromechanical coupling factor K^2=4.5% and effective permittivity $\varepsilon=50\varepsilon_o$.

Input and output transducer capacitance was calculated by applying the technique [16]. Both unapodized and apodized SAW transducer admittances were calculated in terms of the overlap taps using Eq. (3.33). There is good agreement between modeled and measured characteristics in the wide frequency range. The predicted insertion loss value of -19.5 dB agrees well with the measured value of -20 dB.

3.6. Conclusions

The general formula for calculation of the admittance of apodized SAW transducers has been deduced in the quasi-static approximation using nodal admittance matrix of a SAW transducer. By applying a special summation technique for periodic SAW transducers the general formula has been reduced to the compact form resulting in considerable reduction of the computation time if compared to the wide-spread aperture channelizing technique commonly used [11, 12]. According to this formula, the acoustic admittance is given by the Fourier transform of the effective apertures, with effective apertures values being the total overlaps of all the nearest neighbor fingers, next nearest ones, and so on, respectively. Effective apertures are uniquely defined by finger overlaps and do not depend on the frequency. Assumed for a set of the effective apertures to be determined a priori, acoustic admittance

calculation comprising both radiation conductance and susceptance takes no more time than frequency response calculation.

The method is quite general and may be applied to capacitively-weighted, polarity-weighted, multi-phase, and other periodic SAW transducers having the central frequency far away from the synchronous frequency. Results of admittance calculation for SAW transducers with split (double) fingers are presented which agree well with the measured admittance characteristics.

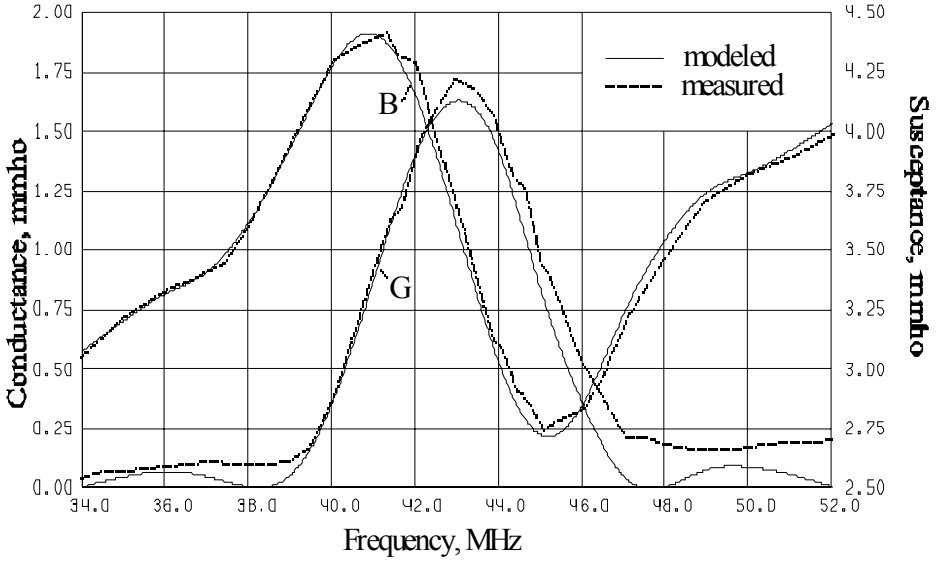

a) input unapodized SAW transducer

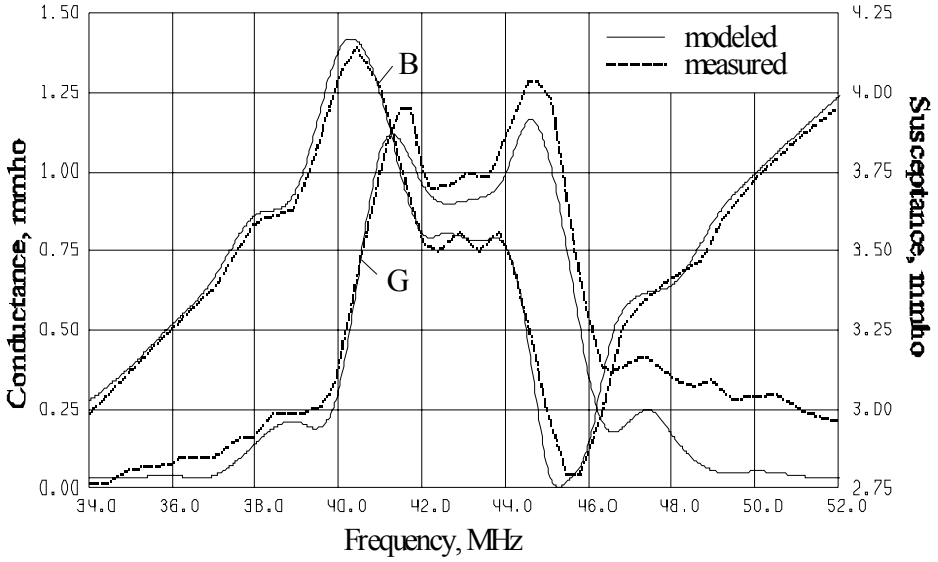

b) output apodized SAW transducer

Fig. 3.4. Modeled and measured admittance characteristics of a SAW bandpass filter

4. STATIC CAPACITANCE CALCULATION FOR PERIODIC SAW TRANSDUCERS

4.1. Statement of the Problem

Properties of SAW interdigital transducers (IDT) can be deduced, to the first order, from the electrostatic solution ignoring piezoelectricity (quasi-static approximation) [4, 5]. Rigorous treatments of the problem for arbitrary finite length IDT based on the Green's function approach are available [5, 8]. However, extensive calculations are necessary to evaluate charge density distribution and/or IDT capacitance by applying point-matching techniques (method of moments [17, 18], for example).

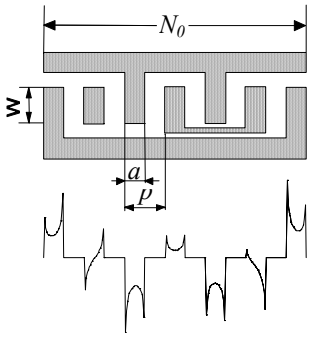

a) without guard fingers

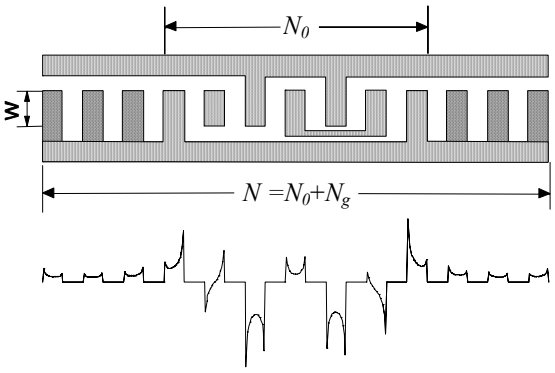

b) with guard fingers

Fig. 4.1. Generalized periodic SAW transducer

Fortunately, in many practical cases an interdigital transducer can be modeled as the periodic array of metallic strips with the arbitrary voltages applied (Fig. 4.1a). The solution is considerably simplified by applying superposition principle [8] and the known analytic solution for the elemental charge density distribution in the infinite periodic single tap transducer having all electrodes grounded, except for the one with unity potential [5-8]. End effects associated with charge density distortion near the ends of a finite length IDT may be suppressed by adding special dummy (guard) grounded fingers at each side of the IDT [5, 8] (Fig. 4.1b).

However, the known solutions in terms of the elemental charge density distribution in the infinite single tap transducer [5-8] suffer from some drawbacks. In general case, the solution includes

complicated integrals of Legendre functions that is inconvenient for practical use. Moreover, there is uncertainty with regard to the number of guard electrodes to be introduced in a real IDT to sufficiently suppress the electrostatic end effects. This number depends on the transducer geometry and tends theoretically to infinity.

Here we follow another approach to model periodic SAW transducers proposed and developed in [14, 16] where the initial electrostatic problem is approximated by an auxiliary one with the periodic boundary conditions on the surface. To this end, an entire IDT containing N electrodes with arbitrary voltages V_i is treated as one generalized period of the infinite periodic array constructed by the sequential multiple replication of the initial transducer (Fig. 4.2). Provided for sufficient uncoupling between adjacent periods due to the special uncoupling grounded (Fig. 4.2a) or floating (Fig. 4.2b) fingers, the solution to be obtained for one period might be a good approximation to the initial problem.

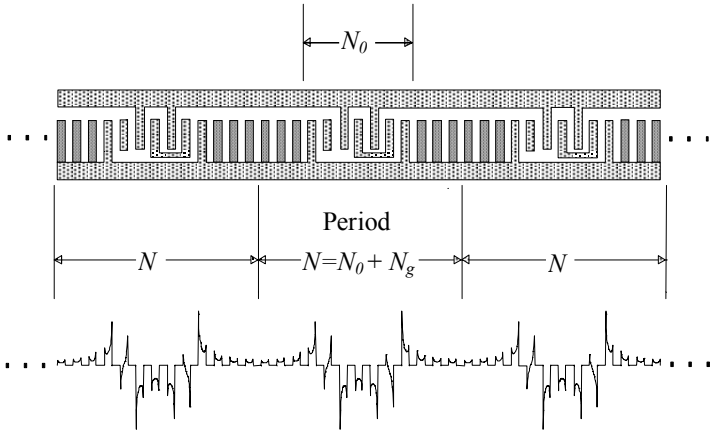

a) connected (grounded) uncoupling electrodes

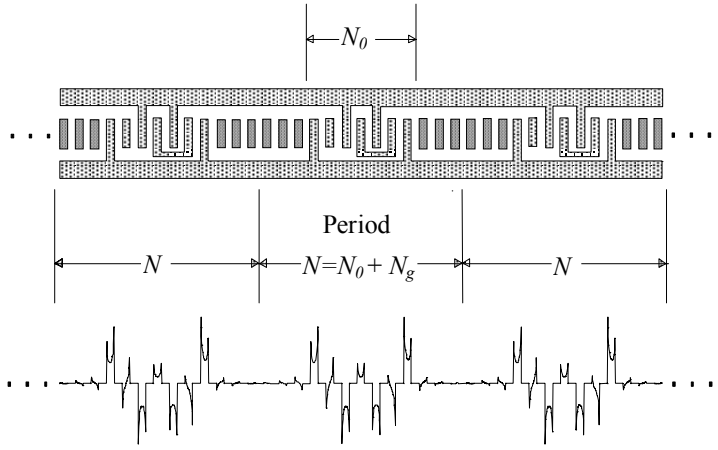

b) disconnected (floating) uncoupling electrodes

Fig. 4.2. Periodic SAW transducer with uncoupling (guard) electrodes

Assumed for all the electrode potentials to be a priori prescribed, the closed-form solution of the auxiliary electrostatic problem can be deduced from the basic charge density distribution in a periodic phased array of the strips [6, 7]. The phased array has the same voltages impressed with the phase progressing uniformly along the array [6, 7]. The solution for one period of the generalized periodic SAW transducer has been found by applying the Floquet's theorem and superposition principle [14,

16]. Results for the infinite periodic arrays [6, 7] follow from the theory as a particular case of the infinite period $N \to \infty$.

The initial electrostatic problem is stated by the electrode geometry of Fig. 4.1 where the basic periodic structure of N_0 strips is considered. All the strips have the uniform width a and fixed pitch p throughout the transducer and hence the constant metallization ratio $\eta=a/p$. The electrodes are allowed to take on any voltages V_i with arbitrary magnitude and phase. It is assumed where appropriate that electrodes are concerned to either of two bus-bars.

An auxiliary periodic structure with connected (grounded) or disconnected (floating) uncoupling fingers is shown in Fig. 4.2. It is worthy noting that floating uncoupling strips in 4.2b allow better uncoupling between adjacent periods as they have zero net charge. However, the presence of the disconnected (floating) strips complicates considerably the problem since their potentials must be beforehand determined. In this chapter, we shall confine our further consideration with the case of the equipotential guard fingers connected to either of the bus-bars.

Therefore, the problem is to determine charge density distribution, net electrode charges, and static capacitance for one generalized period containing $N=N_0+N_g$ electrodes, with N_0 being the number of electrodes in the basic structure and N_g being the total number of the uncoupling (guard) fingers.

4.2. Phased Array Transducer and Basic Analytic Equations

According to the Floquet's theorem for periodic structures, the voltages and charges on the same electrodes of different periods must be the same apart from the phase shift. Therefore, the electrostatic problem should be solved for one generalized period only.

Supposed for all the electrode voltages to be known a priori, a set of the arbitrary voltages on the electrodes can be synthesized as follows

$$V_i = \frac{1}{N}\sum_{s=0}^{N-1}\tilde{V}_s e^{-j\varphi_s i}, \quad \tilde{V}_s = \sum_{i=0}^{N-1} V_i e^{j\varphi_i s}, \quad \varphi_s = 2\pi s / N \tag{4.1}$$

or in matrix form

$$\mathbf{V} = \mathbf{H}\tilde{\mathbf{V}}, \quad \tilde{\mathbf{V}} = \mathbf{H}^{-1}\mathbf{V} \tag{4.2}$$

where $\mathbf{V}=[V_0 V_1 \ldots V_{N-1}]^T$ is vector of the electrode voltages and an auxiliary vector $\tilde{\mathbf{V}} = [\tilde{V}_0\ \tilde{V}_1 \ldots \tilde{V}_{N-1}]^T$ contains voltages on a set of the phased array transducers, each with the same strip voltage $\tilde{V}_s$ and phase progressing uniformly along the array at the rate $\varphi_s=2\pi s/N$ (Fig. 4.3).

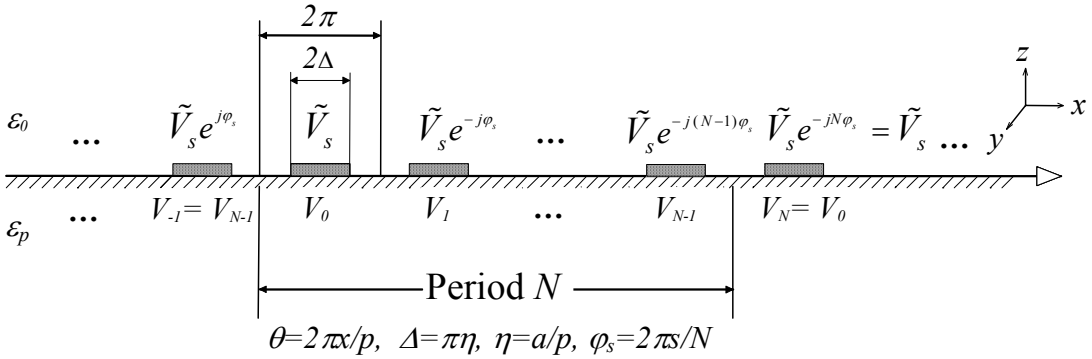

Fig. 4.3. Phased array transducer

The vectors $\mathbf{V}$ and $\tilde{\mathbf{V}}$ are interrelated via a square matrix $\mathbf{H} = [h_{is}]_0^{N-1}$ of the size N with elements $h_{is} = \frac{1}{N} e^{-j\varphi_s i}$. The matrix $\mathbf{H}$ has the closed-form inverse matrix $\mathbf{H}^{-1}=N\ \mathbf{H}^*$ with elements $h_{is} = e^{j\varphi_i s}$ where the asterisk denotes matrix Hermitian conjugation.

The charge distribution in a phased array transducer is known to be of the form [6, 7]

$$\tilde{\sigma}_s(\theta) = \tilde{\gamma}_s(\theta)\, \tilde{V}_s \tag{4.3}$$

$$\tilde{\gamma}_s(\theta) = \frac{2\sqrt{2}\varepsilon}{p} \frac{\sin \pi s/N}{P_{-s/N}(-\cos\Delta)} \frac{e^{-j(s/N-\frac{1}{2})\theta}}{\sqrt{\cos\Delta - \cos\theta}}, \quad |\theta| \le \Delta \tag{4.4}$$

where $\Delta=\pi\eta$; $\varepsilon=\varepsilon_0+\varepsilon_p$ is the surface effective permittivity, ε_0 is permittivity of the medium above the surface; $\varepsilon_p = \sqrt{\varepsilon_{11}\varepsilon_{33} - \varepsilon_{13}^2}$ is the effective permittivity of the substrate; $P_{-s/N}(-\cos\Delta)$ is the Legendre function, and $\theta=2\pi x/p$ denotes a dimensionless variable related to coordinate x.

The total charge on the electrode of a phased array transducer can be found by integrating (4.3), (4.4) over the strip width [6, 7] using the Mehler-Dirichlet's formula [19]

$$\tilde{Q}_s = \tilde{\gamma}_s \tilde{V}_s, \tag{4.5}$$

$$\tilde{\gamma}_s = 2\,\varepsilon \sin \pi s/N \frac{P_{-s/N}(\cos\Delta)}{P_{-s/N}(-\cos\Delta)} \tag{4.6}$$

Thus, according to Eq. (4.1) an arbitrary periodic IDT containing N electrodes in the generalized period can be effectively modeled by superposition of a set of N phased array transducers in terms of the known closed-form solutions (4.3)-(4.6) for the charge distribution in the elemental phased array transducers.

4.3. Surface Charge Density Distribution

By applying the superposition principle (4.1) the charge density distribution on the i-th electrode can be expressed as

$$\sigma_i(\theta) = \frac{1}{N} \sum_{s=0}^{N-1} \tilde{\sigma}_s(\theta) e^{-j\varphi_s i} \tag{4.7}$$

where $\tilde{\sigma}_s(\theta)$ is the charge density distribution in the s-th phased array transducer with the strip voltage $\tilde{V}_s$. By substituting (4.3), (4.4) into (4.7) and taking into account the second Eq. (4.1) we can derive after some manipulations with indexes the following closed-form expression

$$\sigma_i(\theta) = \sum_{p=0}^{N-1} \gamma_p(\theta) V_{i-p}, \tag{4.8}$$

$$\gamma_p(\theta) = \frac{1}{N} \sum_{s=0}^{N-1} \tilde{\gamma}_s(\theta)\, e^{-j2\pi ps/N} \tag{4.9}$$

where the coefficients $\gamma_p(\theta)$ represent the basic charge density distribution on the period of N electrodes with one electrode activated and all others grounded and with the zero index p=0 attributed to the activated finger. According to Eq. (4.8), the charge distribution $\sigma_i(\theta)$ is given by the convolution product of the basic charge distribution $\gamma_p(\theta)$ with the electrode voltages V_i.

As an example, the charge density distributions on one period of the multielectrode periodic Engan's transducers [13] are shown in Fig. 4.4 for N=2, 3, 4, and 6 with different polarity sequences for metallization ratio η=0.5.

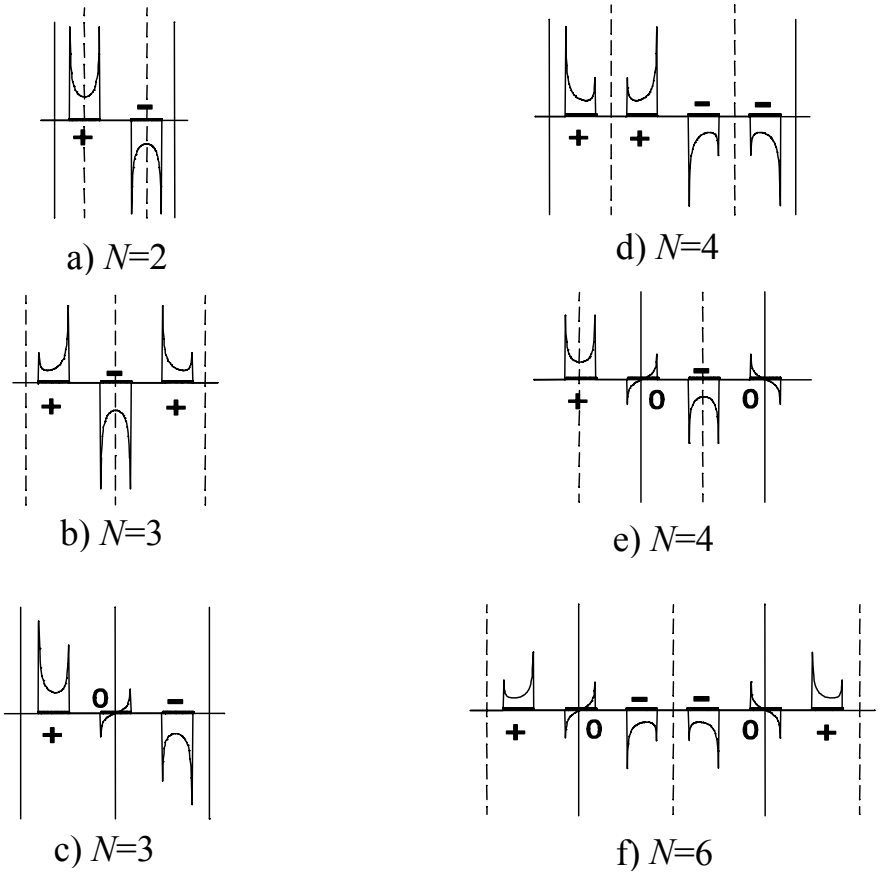

Fig. 4.4. Charge density distribution on one period of the periodic multielectrode Engan's transducers

4.4. Interrelation of Electrode Charges and Voltages. Capacitive and Potential Matrices

By integrating (4.8), (4.9) over the electrode width we deduce the following closed-form relations to express charges in terms of electrode potentials and vice versa [14, 16]:

$$Q_i = \sum_{p=0}^{N-1} \gamma_p V_{i-p}, \quad V_i = \sum_{p=0}^{N-1} \gamma_p^+ Q_{i-p}, \tag{4.10}$$

where

$$\begin{Bmatrix} \gamma_p \\ \gamma_p^+ \end{Bmatrix} = \frac{1}{N} \sum_{s=0}^{N-1} \begin{Bmatrix} \tilde{\gamma}_s \\ \tilde{\gamma}_s^+ \end{Bmatrix} e^{-j2\pi s/N} \tag{4.11}$$

or in matrix form

$$\mathbf{Q} = \mathbf{\Gamma V}\,, \quad \mathbf{V} = \mathbf{\Gamma}^+ \mathbf{Q} \tag{4.12}$$

$$\mathbf{\Gamma} = \mathbf{H}^{-1} \tilde{\mathbf{\Gamma}}\, \mathbf{H}\,, \quad \mathbf{\Gamma}^+ = \mathbf{H}^{-1} \tilde{\mathbf{\Gamma}}^+ \mathbf{H} \tag{4.13}$$

where "+" denotes pseudo-inversion [20] of the matrix $\mathbf{\Gamma}$ which is degenerate due to the charge neutrality condition. The elements of the diagonal matrices $\tilde{\mathbf{\Gamma}}$ and $\tilde{\mathbf{\Gamma}}^+$ are interrelated as $\tilde{\gamma}_s^+ = 1/\tilde{\gamma}_s$, $s \neq 0$ with $\tilde{\gamma}_0^+ = 0$ where the matrix elements $\tilde{\gamma}_s$ are given by Eq. (4.6).

The capacitive matrix $\mathbf{\Gamma}$ relating the electrode charges to voltages has the structure

$$\mathbf{\Gamma} = \begin{bmatrix} \gamma_0 & \gamma_1 & \gamma_2 & \cdots & \gamma_2 & \gamma_1 \\ \gamma_1 & \gamma_0 & \gamma_1 & \cdots & \gamma_1 & \gamma_2 \\ \gamma_2 & \gamma_1 & \gamma_0 & \cdots & \gamma_4 & \gamma_3 \\ \vdots & & & \ddots & & \vdots \\ \gamma_2 & \gamma_3 & \gamma_4 & \cdots & \gamma_0 & \gamma_1 \\ \gamma_1 & \gamma_2 & \gamma_3 & \cdots & \gamma_1 & \gamma_0 \end{bmatrix} \tag{4.14}$$

and the pseudo-inverse potential matrix $\mathbf{\Gamma}^+$ relating voltages to charges has the same structure, with the elements γ_p replaced by the γ_p^+.

The quantities $\gamma_p = \gamma_p(N, \eta)$ are the charges on the electrodes of the basic periodic structure, with only one electrode of the period activated. They are slowly varying functions of the metallization ratio η and fall off rapidly (at a rate of the order $1/p^2$) as the relative electrode number p increases. The coefficients γ_p take the simplest form in the particular case of η=0.5 when $\tilde{\gamma}_s = 2\varepsilon \sin \pi s/N$. In this case, Eq. (4.11) is reduced to the simple analytic formula

$$\gamma_p = 2\varepsilon \frac{\sin p/N}{N\,(\cos 2\pi p/N - \cos p/N)}, \quad p = 0, 1, \ldots, N-1. \tag{4.15}$$

The known results [6, 7] follow from Eqs. (4.11) and (4.6) as the particular limiting case of $N \to \infty$, with the discrete variable s/N replaced by the continuous variable ν and summation replaced by integration:

$$\gamma_p = \int_0^1 \tilde{\gamma}(\nu)\, e^{-j2\pi p\nu} d\nu\,, \quad \tilde{\gamma}(\nu) = 2\varepsilon \sin \pi\nu \frac{P_{-\nu}(\cos\Delta)}{P_{-\nu}(-\cos\Delta)}\,, \quad p = 0, 1, 2, \ldots \tag{4.16}$$

4.5. Static Capacitance of a SAW Transducer

We can deduce an analytic expression for the static capacitance C using the energy conservation law written in the form

$$\frac{1}{2}C\Delta V^2 = \frac{1}{2}\mathbf{V}^*\mathbf{Q} \tag{4.17}$$

where ΔV is the voltage applied to the transducer bus-bars, $\mathbf{V}=[V_0\ V_1\ \dots\ V_{N-1}]^T$ and $\mathbf{Q}=[Q_0\ Q_1\ \dots\ Q_{N-1}]^T$ are vectors of the voltages and charges on the electrodes, respectively. Substitution of the first Eq. (4.12) into (4.17) leads to the following expressions for the capacitance of an unapodized SAW transducer of the unit aperture W=1

$$C = \frac{1}{\Delta V^2}\mathbf{V}^*\mathbf{\Gamma}\,\mathbf{V} = \frac{1}{N\Delta V^2}\tilde{\mathbf{V}}^*\tilde{\mathbf{\Gamma}}\,\tilde{\mathbf{V}} \tag{4.18}$$

or in the scalar form

$$C = \frac{1}{\Delta V^2}\sum_{i=0}^{N-1}\sum_{k=0}^{N-1}\gamma_{ik}V_iV_k = \frac{1}{N}\sum_{s=1}^{N-1}\tilde{C}_s, \quad \tilde{C}_s = \tilde{\gamma}_s\left|\frac{\tilde{V}_s}{\Delta V}\right|^2 \tag{4.19}$$

where the quantities $\gamma_{ik}=\gamma_{|i-k|}$, $i\neq k$ may be interpreted as the charges on the capacitors $C_p=-\gamma_p$, $p=|i-k|$ connected between i-th and k-th electrodes (Fig. 4.5), with γ_0 equal to the total sum of the charges on all capacitors.

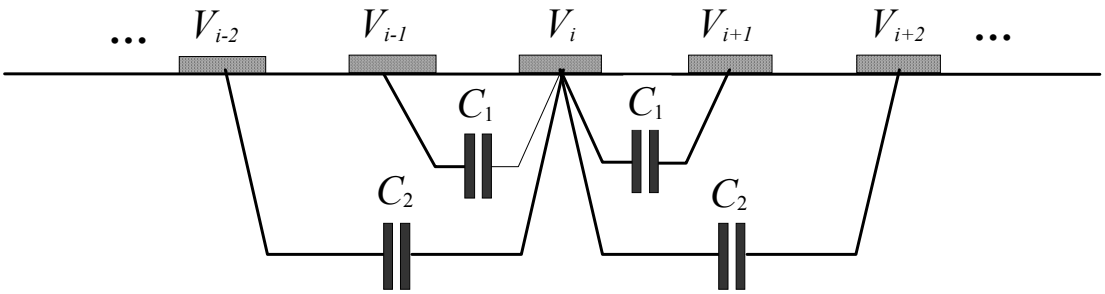

Fig. 4.5. Interelectrode capacitors

By using the identity $2V_iV_k = V_i^2 + V_k^2 - (V_i - V_k)^2$ and the charge neutrality condition within one period

$$\sum_{i=0}^{N-1}\gamma_{ik} = \sum_{k=0}^{N-1}\gamma_{ik} = 0 \tag{4.20}$$

and taking into account the full transducer aperture W, the first Eq. (4.19) may be converted to the form

$$C = -\frac{1}{2}\sum_{i=0}^{N-1}\sum_{k=0}^{N-1}\gamma_{ik}W_{ik} = -\sum_{i=0}^{N-1}\sum_{k=0}^{i-1}\gamma_{ik}W_{ik}\ ,\ W_{ik} = \left(\frac{V_i - V_k}{\Delta V}\right)^2 W \tag{4.21}$$

If each electrode is connected to either of bus-burs ($V_i=\pm\Delta V/2$) then $W_{ik}=0$ for $V_i=V_k$ and $W_{ik}=W$ for $V_i\neq V_k$. Thus, the partial apertures W_{ik} are equal to the overlaps of the i-th and k-th electrodes.

Eq. (4.21) can be converted to the compact form by using the symmetry properties and reordering the summation

$$C = \sum_{p=1}^{N-1}C_pL_p \tag{4.22}$$

where

$$L_p = \sum_{k=0}^{N-1-p} W_{k,k+p} \quad \text{or} \quad L_p = \sum_{k=p}^{N-1} W_{k,k-p}\ , \quad p = 0, N-1 \tag{4.23}$$

The quantities L_p are the total overlaps of all the nearest neighbor electrodes, the next nearest ones, and so on, respectively. Following the same considerations as for the transducer admittance calculation, we can see that the static capacitance is composed of the weighted interelectrode capacitors, with formula (4.23) being applicable both to unapodized and apodized SAW transducers with arbitrary polarity sequences.

The results for the static capacitance calculation agree with those for the transducer admittance calculation in Chapter 3. Eq. (4.22) for the static capacitance has the same form as Eq. (3.30) for the transducer admittance. The weights W_{ik} and the quantities L_p in Eqs. (4.22), (4.23) have basically the same meaning as in the case of the admittance calculation. Therefore, the capacitors $C_p=-\gamma_p$ could be included in the elemental admittances $Y_p=G_p+jB_p+j\omega C_p$. However, this is advantageous to calculate separately the radiation part of the admittance G_p+jB_p and the static capacitance C.

The known Engan's results for the capacitance of multielectrode periodic transducers [13] follow from the second Eq. (4.19) as the particular case for N=2, 3, 4, and 6, with the capacitance values per period given in Table 4.1 for the metallization ratio η=0.5.

Table 4.1

Capacitance of the multielectrode periodic SAW transducers

N	V_k, $k=0,N-1$	$\tilde{\gamma}_1/\varepsilon$	$\left\|\tilde{V}_1/\Delta V\right\|^2$	C/ε
2	+ −	2	1	1
3	+ − +	$\sqrt{3}$	1	$2/\sqrt{3}$
3	+ 0 −	$\sqrt{3}$	3/4	$\sqrt{3}$
4	+ + − −	$\sqrt{2}$	2	$\sqrt{3}/2$
4	+ 0 −0	$\sqrt{2}$	1	$1/\sqrt{2}$
6	+ 0 − − 0 +	1	3	1

4.6. Conclusions

The complete closed-form solution of the electrostatic problem for periodic SAW transducers has been considered in this chapter where IDT is treated as one generalized period of the periodic structure derived by sequential multiple replication of the initial IDT. Special uncoupling grounded fingers (guard electrodes) are introduced to uncouple between adjacent periods while calculating and to suppress end effects in the real finite length IDT.

Known results for infinite periodic arrays follow from the theory as a particular limiting case of the infinite period $N\to\infty$. However, the advantages of the proposed approach are apparent:

1. Physical redundancy of the infinite array is removed.

2. There is a simple criterion (uncoupling between periods) to evaluate a number of the uncoupling fingers to be introduced in the real IDT to suppress end effects.

3. Closed-form expressions are derived in terms of finite summation instead of finite series and integrals.

5. MULTISTRIP COUPLER MODELING: TWO-MODE APPROACH

5.1. Concept of a Multistrip Coupler

A conventional multistrip coupler (MSC) [21-24] consists of an array of the identical metallic strips oriented parallel to the surface acoustic wave wavefront on the surface of the piezoelectric substrate (Fig. 5.1).

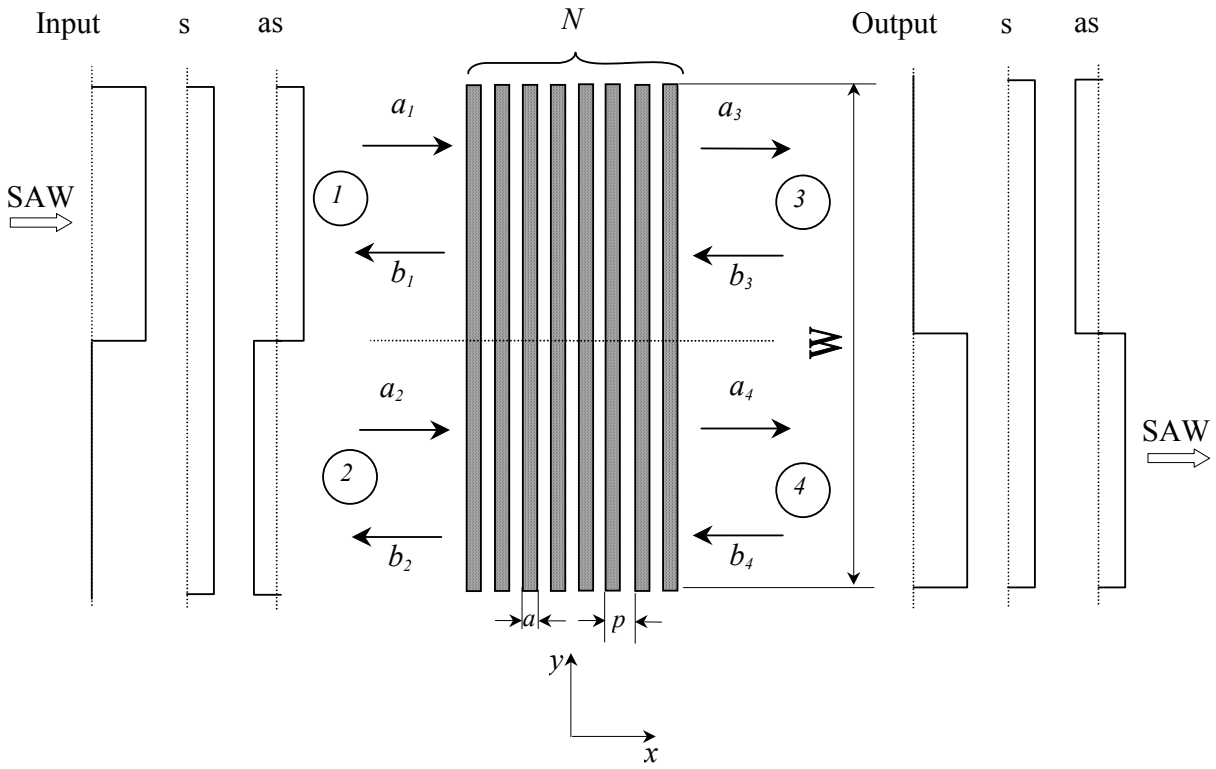

Fig. 5.1. Multistrip coupler and normal mode representation

The major purpose of using the MSC is to transfer laterally the surface power of the acoustic wave incident to one of its ports. The output acoustic wave occupies an adjacent track with respect to the incident input wave. Therefore, in SAW filters the MSC can be used to couple acoustically two interdigital transducers whose active regions do not overlap. This arrangement has the practical merits that 1) two apodized SAW transducers can be used, with the overall SAW filter response easily calculated and 2) spurious signals due to excitation of the bulk waves are much suppressed as only the surface acoustic waves are effectively coupled through a MSC.

The basic MSC mechanism is a straightforward consequence of the piezoelectric effect. A surface wave incident in one track causes voltages induced on the conducting metallic strips. As the strips are assumed to be perfect conductors, the same voltages are applied to in the second track generating a secondary output surface wave. At any frequency, the induced voltages have the same relative phases corresponding to the propagating surface wave, so that the partial waves generated by the strips in the second track are in-phase. One could intuitively anticipate that this should result in a wide bandwidth of the coupler. Therefore, the MSC can be effectively used for acoustic energy transfer

in the wide frequency band. As the number of the MSC strips depends inversely on the piezoelectric coupling of the substrate material [21-24], the application of the MSC is practicable for strongly piezoelectric materials such as lithium niobate, for example.

5.2. Normal Mode Representation of a Multistrip Coupler

The MSC analysis in this chapter is based on the following assumptions:

1) the MSC is periodic with a constant strip width a and pitch (period) p throughout the structure;
2) both acoustic tracks are identical and have equal aperture $W/2$;
3) the width W of the acoustic tracks is much larger than the MSC period p, i.e. $W/p>>1$ so that we can neglect the transversal end effects;
4) number of the MSC strips is sufficiently large to neglect end effects in the finite length MSC;
5) coupling to bulk waves can be neglected;
6) diffraction of the acoustic waves can be neglected;
7) MSC strips are perfectly conducting so that each strip can be considered as the equipotential conductor;
8) surface waves propagate perpendicular to the strips;
9) metal strips are infinitely thin and deposited on a strongly piezoelectric substrate like lithium niobate so that we can neglect interelectrode mechanical reflections due to the mass loading;
10) the frequency range is limited to the baseband including the first stopband.

In common with other coupled-mode systems, a quantitative description can be obtained in terms of the propagating normal modes of the structure which are essentially the solutions where all the field variables such as surface potential $\phi(x)$ have the property $\phi(x+p)\exp(-jkp)$ with k being the wavenumber, so far unknown. By other words, the normal modes of the structure are the acoustic field patterns which are not distorted on propagating through the coupler, with each mode propagating through the coupler independently of others.

We first consider an infinite array ($N\rightarrow\infty$) of regular strips with width a and pitch p. The strip length W in the transversal direction is assumed to be sufficiently large. Therefore, all the field quantities over the strips can be taken to be independent of y. The voltage on the n-th electrode is V_n while the current entering this electrode is I_n. As the structure is periodic with the period p in the x-direction, we can apply the Floquet's theorem to the solutions for the strip voltage and current which take the form

$$V_n = V_0 e^{-jknp} \tag{5.1}$$

$$I_n = I_0 e^{-jknp} \tag{5.2}$$

It is worthy to note that these solutions are unaffected if a multiple of $2\pi/p$ is added to k. The solutions must satisfy to the boundary conditions. Within the model constraints applied, the electrical boundary conditions are as follows:

1) the strip potential and current are continuous at the intersection between two tracks;
2) the net charge on the strip is equal to zero due to the charge neutrality condition;
3) strip current density is equal to zero at the ends of the strip.

The latter is an approximation that neglects the stray field at the end of the strips and the diffracted acoustic field. The contribution from the stray field is negligible when the strips are much longer than the period p and the diffraction is believed to be small for the normal modes.

As a SAW velocity under the structure is slower than the free surface velocity, we may conclude

that the MSC of the finite width W must act as a waveguide. Even in case of the perfectly conducting strips there exist infinite number of the symmetric and antisymmetric orthogonal normal modes of the structure propagating with different phase velocities [25]. For the infinitely wide aperture $W\to\infty$, the normal modes degenerate into two lowest symmetric and antisymmetric rectangular modes. For the wide apertures (say, $W/\lambda>30$), these two modes are dominating. Therefore, the MSC behavior can be modeled in terms of these modes, to a good degree of accuracy. Any input wave pattern that is uniform can be decomposed into these modes as shown in Fig. 5.1.

In general, the symmetric and antisymmetric modes propagate with different velocities v_s and v_{as}, respectively and it is beating of these two modes that leads to a periodic change of energy in the tracks. Particularly, when these two modes are in anti-phase while propagating on the acoustic path the input acoustic energy is transferred from one track to another.

The physical meaning of the symmetric and antisymmetric rectangular modes is rather straightforward and follows from the properties (5.1) and (5.2). We denote the electrode coupled voltages and currents V_n^u, I_n^u and V_n^l, I_n^l for upper and lower tracks of the n-th strip, respectively. As the strips are supposed to be equipotential, the voltages are the same in both tracks

$$V_n^u = V_n^l \qquad .(5.3)$$

On the other hand, as the strips are isolated and both tracks are identical, the charge neutrality condition requires

$$I_n^u = -I_n^l \qquad (5.4)$$

We can define the modes by reference to the coupled voltage and current conditions. The symmetric mode has a uniform amplitude and phase distribution over the strip, i.e. the acoustic potential $\phi_n^u = \phi_n^l$ is the same for both tracks. Therefore, it satisfies to the condition of the zero coupled flux (charge flowing from one half of a strip to another) giving $I_n^u = I_n^l = 0$. As the velocity is the same in each track, amplitude and phase synchronism is maintained during propagation irrespective of whether or not the metal strips are connected at the intersection line separating the tracks. The voltages on the corresponding strips in each track are identical $V_n^u = V_n^l$, whether joined or not. Therefore, no charge flows between them giving the condition of the zero coupled flux. Since there are no charge flows between the tracks, each track supports propagation of the mode as if its electrodes were open-circuited. This is the same as the solution for the open-circuit periodic grating. Consequently, the symmetric mode wave number is $k_s = k_{oc}$ where k_{oc} is the wavenumber in the open-circuit grating.

The antisymmetric mode is defined by the condition of the zero coupled potential. This mode is composed of waves propagating in two tracks in anti-phase. Physically, this is to be expected when the acoustic potentials in the two tracks are equal and opposite, i.e. $\phi_n^u = -\phi_n^l$. Therefore, equal and opposite surface charges would be generated in each strip if they were not joined. By connecting them charges flow and exact charge compensation takes place due to the charge neutrality condition giving $I_n^u = -I_n$. Consequently, no voltage appears at any strip and the condition of the zero coupled potentials $V_n^u = V_n^l = 0$ applies. Since all the strip voltages are equal to zero, each track supports propagation of this mode as if its electrodes were all connected (short-circuited). Therefore, the antisymmetric mode wavenumber is $k_a = k_{sc}$ where k_{sc} is the wavenumber in the short-circuit periodic grating.

Thus, the symmetric and antisymmetric modes are essentially the surface waves propagating in the open- and short-circuit periodic gratings, with their wavenumbers given by k_{oc} and k_{sc}, respectively. This assumption simplifies greatly the MSC analysis as the known results of the theory of periodic gratings can be applied [26, 27].

5.3. Scattering Matrix of a Multistrip Coupler

The MSC scattering matrix **S** relates the amplitudes of the reflected waves b_i with amplitudes of the incident waves a_i, $i = \overline{1,4}$ at the MSC ports

$$\mathbf{B} = \mathbf{SA} \tag{5.5}$$

where $\mathbf{A}=[a_1\ a_2\ a_3\ a_4]^{\mathrm{T}}$ and $\mathbf{B}=[b_1\ b_2\ b_3\ b_4]^{\mathrm{T}}$ are vectors of the incident and reflected waves, respectively, and

$$\mathbf{S} = \begin{bmatrix} s_{11} & s_{12} & s_{13} & s_{14} \\ s_{21} & s_{22} & s_{23} & s_{24} \\ s_{31} & s_{32} & s_{33} & s_{34} \\ s_{41} & s_{42} & s_{43} & s_{44} \end{bmatrix}. \tag{5.6}$$

For the regular MSC shown in Fig. 5.1, all the ports are symmetric and acoustically equivalent. Therefore, by symmetry and reciprocity it follows that the matrix **S** contains only four independent elements, i.e.

$$\mathbf{S} = \begin{bmatrix} s_{11} & s_{12} & s_{13} & s_{14} \\ s_{12} & s_{11} & s_{14} & s_{13} \\ s_{13} & s_{14} & s_{11} & s_{12} \\ s_{14} & s_{13} & s_{12} & s_{11} \end{bmatrix}. \tag{5.7}$$

Supposed for the scattering matrices of the symmetric mode (open-circuit grating propagation) and antisymmetric mode (short-circuit grating propagation) to be known a priori

$$\mathbf{S}^{a,s} = \begin{bmatrix} s_{11}^{a,s} & s_{12}^{a,s} \\ s_{21}^{a,s} & s_{22}^{a,s} \end{bmatrix}, \tag{5.8}$$

we can express the MSC scattering matrix in terms of the scattering coefficients of the modes by applying the appropriate boundary conditions at each port.

Let the wave $a_1=a$ in the upper track be the only incident wave in the system (a_i=0, i=2,3,4). By expansion of the waves in the upper and lower tracks $a_1=a$ and a_2=0 at the left-hand side of the MSC into symmetric and antisymmetric modes we obtain the following boundary conditions in terms of the normal modes

$$\begin{cases} a_1 = a_1^s + a_1^a = a \\ a_2 = a_2^s + a_2^a = 0 \end{cases}. \tag{5.9}$$

As the symmetric mode has the same amplitudes in two tracks $a_1^{\mathrm{s}}= a_2^{\mathrm{s}}$ and the antisymmetric mode has opposite amplitudes $a_1^{\mathrm{a}}=-a_2^{\mathrm{a}}$ we can find the mode amplitudes

$$\begin{cases} a_1^s = \quad a_2^s = a/2 \\ a_1^a = -a_2^a = a/2 \end{cases}. \tag{5.10}$$

Now, we can express the reflected waves b_i in terms of the reflected symmetric and antisymmetric modes which are related with the incident modes through the corresponding scattering coefficients [28, 29]

$$\begin{cases} b_1 = b_1^s + b_1^a = s_{11}^s a_1^s + s_{11}^a a_1^a = \dfrac{1}{2}(s_{11}^s + s_{ss}^a)a_1 \\ b_2 = b_2^s + b_2^a = s_{11}^s a_2^s + s_{11}^a a_2^a = \dfrac{1}{2}(s_{11}^s - s_{ss}^a)a_1 \\ b_3 = b_3^s + b_3^a = s_{21}^s a_1^s + s_{21}^a a_1^a = \dfrac{1}{2}(s_{21}^s + s_{21}^a)a_1 \\ b_4 = b_4^s + b_4^a = s_{21}^s a_2^s + s_{21}^a a_2^a = \dfrac{1}{2}(s_{21}^s - s_{21}^a)a_1 \end{cases} \tag{5.11}$$

From. Eq. (5.11) we find the following MSC scattering coefficients

$$\begin{aligned} s_{11} = s_{22} &= \frac{b_1}{a_1} = \frac{1}{2}(s_{11}^s + s_{11}^a) \\ s_{12} = s_{21} &= \frac{b_2}{a_1} = \frac{1}{2}(s_{11}^s - s_{11}^a) \\ s_{13} = s_{31} &= \frac{b_3}{a_1} = \frac{1}{2}(s_{21}^s + s_{21}^a) = \frac{1}{2}(s_{12}^s + s_{12}^a) \\ s_{14} = s_{41} &= \frac{b_4}{a_1} = \frac{1}{2}(s_{21}^s - s_{21}^a) = \frac{1}{2}(s_{12}^s - s_{12}^a) \end{aligned} \tag{5.12}$$

Thus, the independent elements of the MSC scattering matrix s_{ik} are determined in terms of the scattering matrices for symmetric and antisymmetric modes $s_{ik}{}^s$ and $s_{ik}{}^a$.

Therefore, in the two-mode assumption the problem of MSC analysis is split into two separate tasks:

1) modeling the propagation and scattering of the symmetric and antisymmetric modes which are essentially normal modes of the open- and short-circuit periodic gratings;
2) construction of the MSC scattering matrix (5.7) from the corresponding scattering matrices of the modes using Eq. (5.12).

5.4. Properties of the Normal Modes in the Periodic Gratings

5.4.1. Wavenumber and SAW Velocity

Surface wave propagation in the periodic gratings on the piezoelectric substrate was first investigated in [27, 28] where a concept of the wavenumber-dependent permittivity was applied to the piezoelectric substrate. For the ideally conducting infinitely thin electrodes, the solution for the periodic electric fields was found by applying Floquet's theorem and using Legendre polynomial expansions. Closed-form dispersion relations for the short- and open-circuited electrodes in the

infinitely long periodic structures were deduced within and outside the grating stop-band. The results were further generalized in the weak-coupling approximation [30, 31] that assumes for the incident wave amplitude to be constant while traversing the electrode region. The reflection coefficients of the open- and short-circuit strip in the infinite periodic grating were found in the closed-form in terms of the Legendre function expansion [5].

We start from the equations for the propagation constants in the periodic grating. By applying the general approach [27, 28] to the analysis of SAW propagation, the following equations for the wavenumbers k_{sc} and k_{oc} in the short- and open-circuit electrodes were deduced [5, Eq. (D26, D29)]

$$k_{sc}^2 = k_0^2 + \frac{1}{2}(k_m^2 - k_0^2)\left[1 + \frac{P_\nu(-\cos\Delta)}{P_{-\nu}(-\cos\Delta)}\right] \tag{5.13}$$

$$k_{oc}^2 = k_0^2 + \frac{1}{2}(k_m^2 - k_0^2)\left[1 - \frac{P_\nu(\cos\Delta)}{P_{-\nu}(\cos\Delta)}\right] \tag{5.14}$$

where $k_0=\omega/v_0$ is the free-surface SAW wavenumber and $k_m=\omega/v_m$ is the metallized (electrically shorted) surface SAW wavenumber, with v_0 and v_m being the free- and metallized SAW velocities, respectively. Strictly speaking, in Eqs. (5.13), (5.14) the variable ν in the index of the Legendre function should be equal to $\nu=k_{sc,oc}/2\pi$, so that these equations were transcendental. However, since the Legendre functions vary slowly with ν, a good approximation is obtained by using $\nu\approx k_0/2\pi$ that makes the right-hand side be independent of $k_{sc,oc}$.

The wavenumber difference is given by the following expression

$$k_{sc}^2 - k_{oc}^2 = \frac{k_m^2 - k_0^2}{k_0 p}\frac{2\sin\pi\nu}{P_{-\nu}(-\cos\Delta)P_{-\nu}(\cos\Delta)} \tag{5.15}$$

where the identity for the positive and negative values of the indexes and arguments of the Legendre function

$$P_\nu(\cos\Delta)P_{-\nu}(-\cos\Delta) + P_\nu(-\cos\Delta)P_{-\nu}(\cos\Delta) = \frac{2\sin\pi\nu}{\pi\nu} \tag{5.16}$$

has been used [5, Eq. (C6)].

By using the approximation for the piezoelectric coupling factor

$$K^2 = 2\frac{\Delta v}{v} = 2\frac{v_0 - v_m}{v_0} \approx 2\frac{k_m - k_0}{k_0} \approx \frac{k_m^2 - k_0^2}{k_0^2} \tag{5.17}$$

Eq. (5.15) can be converted to the form

$$k_{sc}^2 - k_{oc}^2 \approx \frac{k_0}{p}K^2\frac{2\sin\pi\nu}{P_{-\nu}(-\cos\Delta)P_{-\nu}(\cos\Delta)}. \tag{5.18}$$

By applying the expansion $\sqrt{1+x} \approx 1 + x/2$, $x \ll 1$ we obtain

$$k_{sc} \approx k_0 + \frac{1}{2}(k_m - k_0)\left[1 + \frac{P_\nu(-\cos\Delta)}{P_{-\nu}(-\cos\Delta)}\right] = k_0\left(1 + \frac{1}{4}K^2\left[1 + \frac{P_\nu(-\cos\Delta)}{P_{-\nu}(-\cos\Delta)}\right]\right) \tag{5.19}$$

$$k_{oc} \approx k_0 + \frac{1}{2}(k_m - k_0)\left[1 - \frac{P_\nu(\cos\Delta)}{P_{-\nu}(\cos\Delta)}\right] = k_0\left(1 + \frac{1}{4}K^2\left[1 - \frac{P_\nu(\cos\Delta)}{P_{-\nu}(\cos\Delta)}\right]\right) \tag{5.20}$$

$$k_{sc} - k_{oc} \approx \frac{k_m - k_0}{k_0 p}\frac{2\sin\pi\nu}{P_{-\nu}(-\cos\Delta)P_{-\nu}(\cos\Delta)} = \frac{K^2}{p}\frac{\sin\pi\nu}{P_{-\nu}(-\cos\Delta)P_{-\nu}(\cos\Delta)} \tag{5.21}$$

Eqs. (5.19)-(5.21) have basically the same form as those originally deduced in [28]. By using the expansion $(1+x)^{-1}\approx 1-x$ we can approximate open- and short-circuit SAW velocities as

$$v_{sc} \approx v_0\left(1 - \frac{1}{4}K^2\left[1 + \frac{P_\nu(-\cos\Delta)}{P_{-\nu}(-\cos\Delta)}\right]\right) \tag{5.22}$$

and

$$v_{oc} \approx v_0\left(1 - \frac{1}{4}K^2\left[1 - \frac{P_\nu(\cos\Delta)}{P_{-\nu}(\cos\Delta)}\right]\right). \tag{5.23}$$

These equations give the closed-form solutions for the open- and short-circuit SAW velocities perturbation due to electrical loading, with the mass-loading neglected.

5.4.2. Reflection Coefficient

In the weak-coupling approximation [5, 29, 30], the reflection coefficients of the strip in the short- and open-circuit gratings are given by

$$r_{sc} = -j\frac{\pi}{2}K^2\nu\left(P_{2\nu}(\cos\Delta) + \frac{P_\nu(-\cos\Delta)}{P_{-\nu}(-\cos\Delta)}P_{-2\nu}(\cos\Delta)\right) \tag{5.24}$$

$$r_{oc} = -j\frac{\pi}{2}K^2\nu\left(P_{2\nu}(\cos\Delta) - \frac{P_\nu(\cos\Delta)}{P_{-\nu}(\cos\Delta)}P_{-2\nu}(\cos\Delta)\right) \tag{5.25}$$

It is assumed in Eqs. (5.24), (5.25) that the reflection center is placed in the strip center. In this case the reflection coefficient is imaginary and proportional to the piezoelectric coupling factor K^2 and the normalized frequency ν. It has been shown in Chapter 1 that for a lossless two-port network the reflection and transmission coefficients r and t are interrelated as

$$\begin{cases} |r|^2 + |t|^2 = 1 \\ rt^* + tr^* = 0 \end{cases}. \tag{5.26}$$

It follows from the second Eq. (5.26) that

$$r/t = \pm j\,|r/t|, \tag{5.27}$$

i.e. the coefficients r and t are in phase quadrature [5]. Therefore, the transmission coefficient $t=t^*$ is real when referenced to the strip center. Apart from a phase ambiguity of π, the transmission coefficient t can be deduced from the reflection coefficient r as $t = \pm\sqrt{1-|r|^2}$.

5.4.3. Dispersion Relation for Stopband Propagation

We consider an array of the identical electrodes of width a and period (pitch) p. All the electrodes are either short-circuit or open-circuit ones. In general case, we can find a propagation constant so far unknown by applying the following approach based on the scattering matrix of the elemental cell (Fig. 5.2).

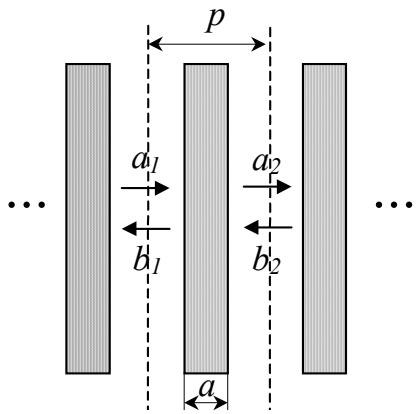

Fig. 5.2. Elemental cell of the periodic grating

As all the elemental cells are identical, all electrodes scatter surface waves in the same manner. We can consider one particular electrode in an array characterized by its reflection and transmission coefficients r and t which are different for the short- and open-circuit cases.

At some frequency ω, it is assumed that the disturbance in the gaps between the electrodes includes terms of the form $\exp(\pm jk_0x)$ representing propagating waves where k_0 is the free-surface wave-number. We denote the right-propagating waves by a_i and the left-propagating wave by b_i, i=1,2 where the subscript 1 is attributed to the waves on the left side and the subscript 2 to the waves on the right side. The reference planes are placed at the points distant half-period $p/2$ from the electrode center. The wave amplitudes are linearly related, so that the waves leaving the electrode can be written in terms of the incident waves using the scattering matrix as

$$\begin{bmatrix} b_1 \\ a_2 \end{bmatrix} = \begin{bmatrix} s_{11} & s_{12} \\ s_{21} & s_{22} \end{bmatrix} \begin{bmatrix} a_1 \\ b_2 \end{bmatrix} \tag{5.28}$$

where $s_{11} = s_{22} = re^{-jk_0p}$ and $s_{12} = s_{21} = te^{-jk_0p}$. If the electrode did not perturb the wave we would have r=0 and $t = e^{-jk_0p}$ (quasi-static approximation). By applying Eq. (1.31) from Chapter 1 we can convert the scattering matrix $\mathbf{S} = [s_{ik}]$, i,k=1,2 to the transmission matrix $\mathbf{T} = [t_{ik}]$, i,k=1,2 relating the waves on the left and right side of the electrode

$$\begin{bmatrix} a_1 \\ b_1 \end{bmatrix} = \begin{bmatrix} t_{11} & t_{12} \\ t_{21} & t_{22} \end{bmatrix} \begin{bmatrix} a_2 \\ b_2 \end{bmatrix} \tag{5.29}$$

Please note that our definition of the transmission matrix **T** differs from the definition given in [5] as it relates the waves at the left to the waves at the right. Such a definition is more convenient for cascading.

The matrix **T** has the following structure

$$\mathbf{T}=\begin{bmatrix} t_{11} & t_{12} \\ t_{21} & t_{22} \end{bmatrix}=\begin{bmatrix} \dfrac{1}{s_{21}} & -\dfrac{s_{22}}{s_{21}} \\ \dfrac{s_{11}}{s_{21}} & s_{12}-\dfrac{s_{11}s_{22}}{s_{21}} \end{bmatrix}=\begin{bmatrix} \dfrac{1}{\tau} & -\dfrac{r}{t} \\ \dfrac{r}{t} & \dfrac{1}{\tau^*} \end{bmatrix} \tag{5.30}$$

where $\tau = te^{-jk_0 p}$ and the properties (5.26) were used. In an infinite lossless array propagating waves at the left and right sides of the electrode should be the same apart from the phase shift

$$\begin{cases} a_1 = a_2 e^{j\gamma p} = 1/\tau a_2 - r/t\, b_2 \\ b_1 = b_2 e^{j\gamma p} = r/t\, a_2 + 1/\tau^* b_2 \end{cases} \tag{5.31}$$

Eq. (5.31) can be rewritten in the equivalent matrix form as

$$\begin{bmatrix} 1/\tau - e^{j\gamma p} & -r/t \\ r/t & 1/\tau^* - e^{j\gamma p} \end{bmatrix}\begin{bmatrix} a_2 \\ b_2 \end{bmatrix}=\mathbf{0} \tag{5.32}$$

where γ is the propagation constant. By equating the determinant of the system (5.32) to zero and using (5.26), we obtain a dispersion relation for γ

$$2\cos\gamma p = \frac{1}{\tau}+\frac{1}{\tau^*} = 2\,\mathrm{Re}\frac{1}{\tau}. \tag{5.33}$$

If the transmission coefficient t is real, the Eq. (5.33) takes the form

$$\cos\gamma p = \frac{\cos k_0 p}{|t|} \tag{5.34}$$

The solution of Eq. (5.34) is given by

$$\gamma p = \pm\arccos\frac{\cos kp}{|t|} + 2\pi n,\ n = 0,1,... \tag{5.35}$$

Outside the stopband $|t|\approx 1$ and the solution of Eq. (5.34) gives the real value $\gamma \approx k_0$. However, in the stop-band $|t|<1$ and the right side of Eq. (5.34) is greater than 1 (or less than –1) when $k_0 p$ is close to a multiple of π. In this case, γ is the complex-valued function $\gamma=\pm\beta+j\alpha$, $\mathrm{Im}\{\alpha\}<0$ giving a stop-band propagating where β is the wave number and α is the attenuation factor. Within any interval of width $2\pi/p$ there exist two solutions for γ corresponding to counter-propagating waves as might be anticipated from physical considerations. For any particular solution in the stop-band, it involves two waves propagating in both directions, even though the overall wave motion is in one direction.

Thus, we derived all the required relations to characterize symmetric (open-circuit) and antisymmetric (short-circuit) modes, in particular:

1) open- and short-circuit wavenumbers k_{oc} and k_{sc} for wave propagation outside the stop-band;
2) dispersion equations for propagation constants γ_{oc} and γ_{sc} in the stop-band;
3) scattering coefficients $r_{oc,sc}$ and $t_{oc,sc}$ (the reflection and transmission coefficients) of one strip in the perioic grating.

5.5. Multistrip Coupler Models

5.5.1. Reflective Array Model (RAM)

Reflective array model is based on the closed-form cascading of the identical elemental reflective cells for an array of N electrodes [5, Appendix E], with the transmission matrix of the array given by $\mathbf{T}^N$ where $\mathbf{T}$ is the transmission matrix (5.30) of one elemental cell. As was shown in [32, 33], the N-th power of the transmission matrix $\mathbf{T}$ is given by the following closed –form equation

$$\mathbf{T}_N = \mathbf{T}^N = P_N(\theta)\mathbf{T} - P_{N-1}(\theta)\mathbf{E} \tag{5.36}$$

where $P_N(\theta)$ is Chebyshev polynomial of the second kind, $\mathbf{E}$ is the unit (identity) matrix, $\theta=2\cos\gamma p$ is the trace of the matrix $\mathbf{T}$ where γ is the propagation constant found from the dispersion equation (5.33). The Chebyshev polynomials can be found in the closed-form from the recurrent relation [32]

$$P_N(\theta) = \frac{\sin N\varphi}{\sin\varphi}, \quad \varphi = \gamma p . \tag{5.37}$$

Therefore Eq. (5.36) takes the form

$$\mathbf{T}_N = \frac{\sin N\varphi}{\sin\varphi}\mathbf{T} - \frac{\sin(N-1)\varphi}{\sin\varphi}\mathbf{E} \tag{5.38}$$

or after substitution of Eq. (5.30) we obtain

$$\mathbf{T}_N = \begin{bmatrix} \frac{1}{\tau}\frac{\sin N\varphi}{\sin\varphi} - \frac{\sin(N-1)\varphi}{\sin\varphi} & -\frac{r}{t}\frac{\sin N\varphi}{\sin\varphi} \\ \frac{r}{t}\frac{\sin N\varphi}{\sin\varphi} & \frac{1}{\tau^*}\frac{\sin N\varphi}{\sin\varphi} - \frac{\sin(N-1)\varphi}{\sin\varphi} \end{bmatrix} \tag{5.39}$$

The transmission matrix $\mathbf{T}_N$ can be converted to the scattering matrix $\mathbf{S}_N$ using Eq. (1.32) applied to the passive grating (V=0)

$$\mathbf{S}_N = \begin{bmatrix} \frac{r}{t}\frac{\tau\sin N\varphi}{\sin N\varphi - \tau\sin(N-1)\varphi} & \frac{\tau\sin\varphi}{\sin N\varphi - \tau(N-1)\sin\varphi} \\ \frac{\tau\sin\varphi}{\sin N\varphi - \tau(N-1)\sin\varphi} & \frac{r}{t}\frac{\tau\sin N\varphi}{\sin N\varphi - \tau\sin(N-1)\varphi} \end{bmatrix}. \tag{5.40}$$

The closed-form scattering matrix $\mathbf{S}_N$ can be used for the symmetric/antisymmetric normal mode description, with the pertinent values of the reflection coefficients $r_{oc,sc}$ and the propagation constants $\gamma_{oc,sc}$ substituted into (5.40).

5.5.2. Coupling-of-Modes (COM) Model

5.5.2.1. COM-Equations and Solutions

The coupling-of-modes (COM) approximation is a closed-form technique to model systems with spatially or time varying properties [34] which has been successfully applied to modeling SAW

gratings and transducers [35, 36].

Consider two counter-propagating waves $a(x)$ and $b(x)$ which can be written in the form

$$\begin{aligned} a(x) &= A(x)e^{-j\frac{K}{2}x} \\ b(x) &= B(x)e^{+j\frac{K}{2}x} \end{aligned} \tag{5.41}$$

where $A(x)$ and $B(x)$ are slowly varying complex amplitudes, $K=2\pi/p$ is the grating wavenumber and p is the pitch of a uniform SAW grating. In the presence of a SAW reflective array, the counter propagating waves get coupled with each other near the Bragg frequency. As the result, the free-surface propagation constant k_o is perturbated by Δk.

COM equations for the reflective array take the form [35, 36]

$$\frac{d}{dx}\begin{bmatrix} A \\ B \end{bmatrix} = \begin{bmatrix} j\delta & j\kappa \\ -j\kappa^* & j\delta \end{bmatrix}\begin{bmatrix} A \\ B \end{bmatrix} \tag{5.42}$$

where $\delta=k_o+\Delta k-K/2$ is the detuning parameter, κ is the coupling factor which characterizes reflectivity per electrode. These two COM-parameters are to be determined (or known) a priori. In general case, the COM parameters depend on frequency, substrate and electrode material as well as on the grating geometry (metallization ratio, pitch, metal film height).

Assumed for simplicity that $\kappa=\kappa^*$ is the real function, the closed-form solution of the system of homogeneous differential equations (5.42) is given by

$$\begin{aligned} A(x) &= h_1 e^{-j\gamma x} + Ph_2 e^{+j\gamma x} \\ B(x) &= Ph_1 e^{-j\gamma x} + h_2 e^{+j\gamma x} \end{aligned} \tag{5.43}$$

where the following notation was introduced

$$\gamma = \sqrt{\delta^2 - \kappa^2}\,,\ P = \frac{\kappa}{\delta+\gamma} = \frac{\delta-\gamma}{\kappa} \tag{5.44}$$

The coefficients h_1 and h_2 are to be determined from the boundary conditions imposed on the incident and reflected waves at the beginning and the end of the finite length grating consisting of N electrodes. If there is the only incident wave of the unit amplitude at the left port, the boundary conditions are as follows

$$\begin{cases} a(0) = 1 \\ b(Np) = 0 \end{cases} \tag{5.45}$$

Substitution of Eqs. (5.41), (5.43) into the system of boundary conditions (5.45) gives

$$h_1 = \frac{1}{1 - P^2 e^{-2jN\varphi}}\,, \qquad h_2 = -\frac{Pe^{-2jN\varphi}}{1 - P^2 e^{-2jN\varphi}} \tag{5.46}$$

where $\varphi=\gamma p$ is the phase shift per period of the grating. By substituting Eqs. (5.46) into (5.43) for $x=0$ and $x=Np$ we obtain the scattering matrix of the grating

$$\mathbf{S} = \begin{bmatrix} R & T \\ T & R \end{bmatrix} \tag{5.47}$$

where the reflection coefficient of the grating

$$R = \frac{b(0)}{a(0)} = \frac{B(0)}{A(0)} = P\,\frac{1 - e^{-2\,jN\varphi}}{1 - P^2 e^{-2\,jN\varphi}} \tag{5.48}$$

and the transmission coefficient

$$T = \frac{a\,(Np)}{a\,(0)} = \frac{A\,(Np)}{A\,(0)} = \frac{1 - P^2}{1 - P^2 e^{-2\,jN\gamma}}\, e^{-jN\varphi} \tag{5.49}$$

5.5.2.2. Determination of COM Parameters

According to Eq. (5.42) there are two principal COM-parameters: wavenumber perturbation $\Delta k = k - k_0$ and the coupling factor κ. For a particular substrate material and grating geometry, the values of these parameters should be determined a priori either numerically or analytically. It is shown in [36] that the fractional wavenumber perturbation $\Delta k/k_0$ can be approximated as follows

$$\Delta k / k_0 = -\frac{\Delta v / v_0}{1 + \Delta v / v_0} \approx -\Delta v / v_0\,, \quad \Delta v / v_0 << 1 \tag{5.50}$$

where $\Delta v = v - v_0$ is the velocity change in the grating. According to Eq. (5.50) the fractional wavenumber perturbation $\Delta k/k_0$ is approximately equal to the fractional velocity change $\Delta v/v_0$ taken with the minus sign. For strongly piezoelectric materials that is the very case for using MSC, we can apply the closed-form Eqs. (5.19), (5.20) or (5.22), (5.23), to a sufficient accuracy. A simple linear approximation can be also used for SAW velocity approximation

$$v \approx (1 - \eta) v_0 + \eta v_m = v_0 (1 - \frac{1}{2} K^2 \eta) \tag{5.51}$$

and hence

$$\frac{\Delta v}{v_0} \approx -\frac{1}{2} K^2 \eta \tag{5.52}$$

where v_0, v_m are the free- and metallized surface SAW velocities, respectively, η is the metallization ratio, K^2 is the piezoelectric coupling factor.

To understand a physical meaning of the coupling coefficient κ, we consider one elemental cell (N=1) of the periodic grating at synchronism (δ=0). In this case COM-variables (5.44) take the values

$$\gamma = j\kappa, \quad P = \kappa / \gamma = -j \tag{5.53}$$

After substituting (5.53) into COM-equation (5.48), we obtain for N=1

$$R = -j\,\frac{1 - e^{-2\,j\gamma p}}{1 + e^{-2\,j\gamma p}} = \tan \gamma p = \tan j\kappa p = j \tanh \kappa p \approx j\kappa p, \quad |\,\kappa p\,| \ll 1 \tag{5.54}$$

On the other hand, according to Eq. (5.28)the reflection coefficient at the synchronous frequency takes

the value

$$R = re^{-j\pi} = -r \tag{5.55}$$

Comparing Eqs. (5.54) and (5.55) we obtain the relationship

$$r = -j\kappa p\,. \tag{5.56}$$

Thus, the coupling factor $\kappa = jr/p$ is the strip reflectivity per unit length of the period. Eq. (5.56) agrees with that deduced in [29].

The COM-parameters can be also deduced from the dispersion curve of the grating which must be calculated or determined experimentally in the proximity of the resonant frequency [38] (Fig. 5.3).

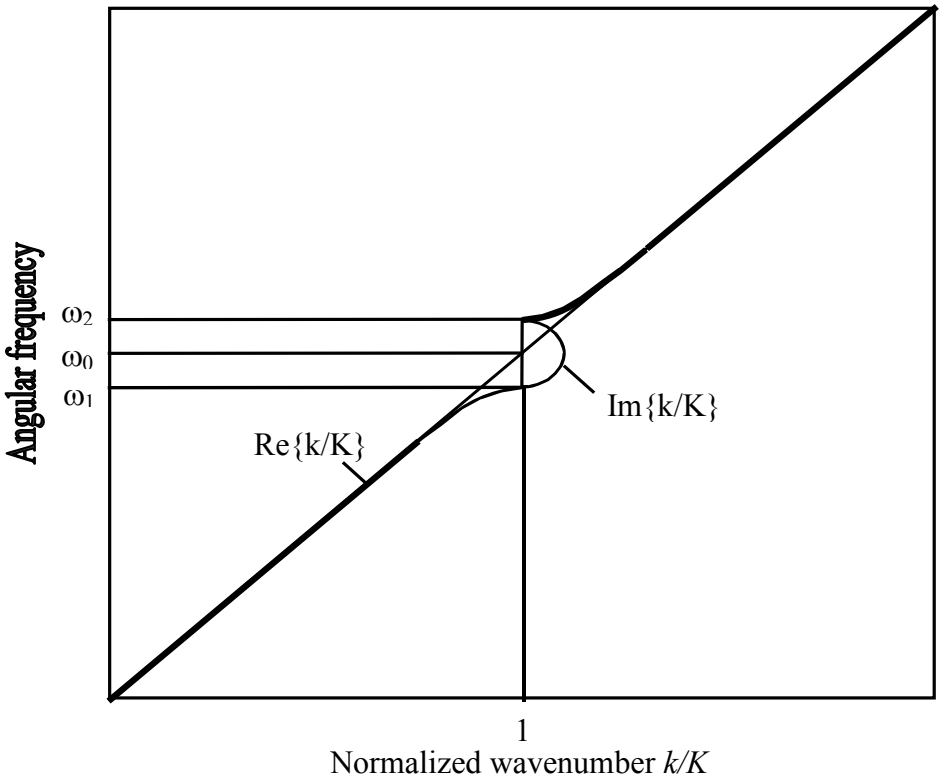

Fig. 5.3. Dispersion curve of the periodic grating

The COM parameters Δk and κ can be deduced from two eigen-frequencies ω_1 and ω_2 which are the stopband frequencies of a periodic short-circuit or open-circuit grating. These frequencies ω_1 and ω_2 degenerate to one single frequency ω_0 for the free surface. From a set of these three frequencies ω_0, ω_1, and ω_2 the wavenumber perturbation parameter Δk can be determined as

$$\frac{\Delta k}{k_0} = -\frac{\omega_1 + \omega_2 - 2\omega_0}{2\omega_0} = 1 - \frac{\omega_1 + \omega_2}{2\omega_0} \tag{5.57}$$

The reflection coefficient per one finger κ is proportional to the stopband width [5]

$$|\kappa| p = \pi \frac{\omega_2 - \omega_1}{\omega_0} \tag{5.58}$$

If all COM parameters are determined, few experiments are required to tune the model if necessary.

5.5.3. Field Approach

The basic idea of the field approach to modeling finite length gratings and MSC is the following [28].

An arbitrary excitation of a finite array can be described in terms of the normal modes. The problem is then to match the normal-mode fields in the array to the fields of the incoming and outcoming (reflected) waves on the free surface outside the array. This can be done approximately at the edges of the array without including volume waves and evanescent modes. We shall use one-dimensional approximation that gives good agreement with experimental data, provided for the transversal length of the electrode (acoustic aperture) being much wider than period p, i.e. $W/p>>1$.

As is known [26, 27], the dominating part of the acoustic power is carried by the fundamental and the first backward harmonics. We can neglect the higher harmonics assuming that they are matched into evanescent modes. Therefore, an acoustic field pattern in a normal-mode excitation of a finite length grating can be written as

$$\phi(x) = a_0 e^{-jkx} + a_{-1} e^{j(K-k)x} + b_0 e^{jkx} + b_{-1} e^{-j(K-k)x} \tag{5.59}$$

where $K=2\pi/p$ is the grating wavenumber, a_0 and a_{-1} are phenomenological wave amplitudes for the fundamental and the first negative spatial harmonics of a forward-running wave, and b_0 and b_{-1} are defined similarly for a backward-running wave. If a_0, b_0 and a_{-1}, b_{-1} are defined as the square root of the total power carried by the fundamental and first negative spatial harmonics, respectively, we obtain the following ratio [28, 37]

$$\rho = \rho(k) = \frac{a_{-1}}{a_0} = \frac{b_{-1}}{b_0} = \frac{k - k_1}{K - k - k_1} \tag{5.60}$$

where ρ is the coupling factor of the fundamental and the first negative spatial harmonics, k is the fundamental wave number and the wavenumber k_1 is defined as

$$k_1 = k_0 \left[1 + \frac{1}{4} K^2 \left(1 - \cos\Delta \right) \right] \tag{5.61}$$

Since k is close to k_1, the ratio (5.60) is close to zero except for the case when k is close to $K/2$ that corresponds to the stop-band propagation. The wavenumber k is supposed to be found from the dispersion equation for the open- or short-circuit grating.

Now, the acoustic field (5.59) must be matched to the incoming and reflected waves at the ends of the array. The boundary conditions at the ends of the array are established by requiring that the incoming wave shall match the waves in the array with phase velocity in the same direction and the waves in the array with phase velocity in the opposite direction shall match the reflected waves.

If there is the only incident wave of the unit amplitude at the left port, the boundary conditions at the edges of the array are as follows

$$\begin{cases} a_0 + \rho b_0 = 1 \\ \rho a_0 e^{-N} + b_0 e^{N} = 0 \end{cases} \tag{5.62}$$

where $e = e^{j\varphi}$, $\varphi = kp$ is the phase lag per period. From the solution of Eq. (5.62) we can find the coefficients

$$a_0 = \frac{1}{1-\rho^2 e^{-2N}}, \qquad b_0 = -\rho a_0 e^{-2N} = -\frac{\rho e^{-2N}}{1-\rho^2 e^{-2N}} \tag{5.63}$$

On the other hand, from Eq. (5.59) the reflected waves at the left and right ports are

$$\begin{cases} B_1 = \rho a_0 + b_0 = \rho(1-e^{-2N})a_0 \\ B_2 = a_0 e^{-N} + \rho b_0 e^{N} = (1-\rho^2)e^{-N} a_0 \end{cases} \tag{5.64}$$

For the unit amplitude of the incident wave, the amplitudes of the reflected waves B_1 and B_2 define the reflection and transmission coefficients R and T, respectively. After substitution of a_0 from Eq. (5.63) into (5.64) we find

$$R = \rho \frac{1-e^{-2jN\varphi}}{1-\rho^2 e^{-2jN\varphi}} \tag{5.65}$$

$$T = \frac{1-\rho^2}{1-\rho^2 e^{-2jN\varphi}} e^{-jN\varphi} \tag{5.66}$$

Eqs. (5.65) and (5.66) can be used for modeling the normal modes in the open- and short-circuit gratings, provided for the wavenumbers k_{oc} and k_{sc} substituted and the harmonic coupling factor $\rho_{oc,sc}$ is defined by Eq. (5.60) The wavenumbers k_{sc} and k_{oc} are determined analytically or found from the dispersion relations. Given the reflection coefficients r_{oc} and r_{sc}, the dispersion equation (5.34) can be used to find the wavenumbers k_{sc} and k_{oc}. Since they are complex-valued function in the stop-band, the harmonic coupling factor ρ is real outside the passband and imaginary in the stop-band.

Another form of the open and short-circuit dispersion relations is based on the expansion to space harmonics [28], with the following approximation applied to the wavenumber k so far unknown

$$k = k_{sc,oc} + \rho(k)\Delta k_{sc,oc}, \tag{5.67}$$

where $k_{sc,\,oc}$ are given by Eqs. (5.19) and (5.20), $\rho(k)$ is given by Eq. (5.60), and

$$\Delta k_{sc} = \frac{1}{4} K^2 k_0 \left(\cos\Delta + \frac{P_{1-\nu}(-\cos\Delta)}{P_{-\nu}(-\cos\Delta)} \right) \tag{5.68}$$

$$\Delta k_{oc} = \frac{1}{4} K^2 k_0 \left(\cos\Delta - \frac{P_{1-\nu}(\cos\Delta)}{P_{-\nu}(\cos\Delta)} \right) \tag{5.69}$$

Eqs. (5.67) are higher order approximations of the wavenumbers for the open- and short-circuit gratings taking into account the first negative spatial harmonic, with the last terms representing the coupling to this harmonic. It is worthy to note that Eqs. (5.19) and (5.20) accounts for only the

fundamental harmonic and follow from Eqs. (5.67) as the particular case ρ=0.

Eqs. (5.67) are transcendental with respect to the wavenumber k and the solutions should be found numerically. However, we can find the closed-form solution by replacing the variable k in the slowly varying functions $k_{sc,oc}$ and $\Delta k_{sc,oc}$ by k_0. In this case Eq. (5.67) can be converted to the following quadratic equation with respect to k

$$k^2 - (K - k_1 + k_{sc,oc} - \Delta k_{sc,oc})k + k_{sc,oc}(K - k_1) - k_1 \Delta k_{sc,oc} = 0 \tag{5.70}$$

The physical solution must be selected of two roots to satisfy the conditions $\mathrm{Re}\{k\}<k_0$ and $\mathrm{Im}\{k\}<0$. Small iteration is required if one wishes to refine the solution. To this end, the found value of the wavenumber k can be substituted into the functions $k_{sc,oc}$ and $\Delta k_{sc,oc}$ and the refined value of k is recalculated using Eq. (5.70).

By substituting the found wavenumbers k and the harmonic coupling factor $\rho(k)$ into Eqs. (5.65) and (5.66) we find the scattering matrices of the open- and short-circuit gratings required for the two-mode MSC analysis using Eqs. (5.12).

5.5.4. Quasi-Static Approximation

In the quasi-static approximation [5], the perturbation of a propagating surface acoustic wave by a shorted electrode is ignored (r=0, $|t|$=1). This model can be treated as a particular (non-reflective) case of the more accurate reflective models discussed previously. It is clear that the quasi-static approximation fails to predict a stop-band propagation. However, outside the stop-band this approximation gives accurate closed-form results in many practical cases. In the standard applications, MSC operates outside the stop-band, so that useful properties and relations can be deduced in the quasi-static approximation.

The shorted electrodes perturb SAW velocity due to the mass-electrical loading effect. For strongly piezoelectric materials, such as lithium niobate, mechanical loading is not significant, provided the metal film used for depositing the metal strips has elastic properties similar to the substrate (this condition is usually met by using the aluminum film). Electrical loading perturbation may cause a considerable change in the SAW velocity. This effect also cannot be accurately modeled in the quasi-static approximation. However, despite the quasi-static approximation is based on the assumption that the wavenumber in the short-circuit grating $k_{sc}\approx k_0$ is essentially the same as the free-surface wavenumber k_0 it predicts to a sufficient accuracy the wavenumber difference for the short- and open-circuit gratings [5, Eq. (5.23)]

$$k_{sc}^2 - k_{oc}^2 = \frac{k_0}{p} K^2 \frac{2\sin\pi\nu}{P_{-\nu}(-\cos\Delta)P_{-\nu}(\cos\Delta)} P_n^2(\cos\Delta) \tag{5.71}$$

or taking into account $k_{sc}+ k_{oc} \approx 2k_0$

$$k_{sc} - k_{oc} \approx \frac{K^2}{p} \frac{\sin\pi\nu}{P_{-\nu}(-\cos\Delta)P_{-\nu}(\cos\Delta)} P_n^2(\cos\Delta) \tag{5.72}$$

where $P_n(\cos\Delta)$ is the Legendre polynomial, n is the space harmonic number. It is surprising that the approximate Eq. (5.71) gives the same result as the accurate formula (5.18).

We suppose for the moment that short- and open-circuit wavenumbers values k_{sc} and k_{oc} are known. In the quasi-static approximation, the scattering matrices of the short- open-circuit gratings are given by

$$\mathbf{S}^{sc,oc} = \begin{bmatrix} 0 & e^{-jNk_{sc,oc}p} \\ e^{-jNk_{sc,oc}p} & 0 \end{bmatrix} \tag{5.73}$$

where for the finite length grating we can neglect end effects if the number N of the strips is sufficiently large. The input and output reference planes are located at the beginning of the first elemental cell and at the end of the last elemental cell, respectively.

After substitution of the normal mode wavenumbers $k_s=k_{oc}$ and $k_a=k_{sc}$ and normal mode scattering coefficients (5.73) into Eqs. (5.12) we obtain the following MSC scattering coefficients

$$\begin{aligned} s_{11} &= \frac{1}{2}(s_{11}^s + s_{11}^a) = \frac{1}{2}(s_{11}^{oc} + s_{11}^{sc}) = 0 \\ s_{12} &= \frac{1}{2}(s_{11}^s - s_{11}^a) = \frac{1}{2}(s_{11}^{oc} - s_{11}^{sc}) = 0 \\ s_{13} &= \frac{1}{2}(s_{12}^s + s_{12}^a) = \frac{1}{2}(s_{12}^{oc} + s_{12}^{sc}) = e^{-jkNp}\cos\frac{N}{2}\Delta kp = e^{-jkNp}\cos\frac{\pi}{2}\frac{N}{N_0} \\ s_{14} &= \frac{1}{2}(s_{12}^s - s_{12}^a) = \frac{1}{2}(s_{12}^{oc} + s_{12}^{sc}) = je^{-jkNp}\sin\frac{N}{2}\Delta kp = je^{-jkNp}\sin\frac{\pi}{2}\frac{N}{N_0} \end{aligned} \tag{5.74}$$

where $k = \dfrac{k_{sc} + k_{oc}}{2}$ can be treated as the MSC wavenumber, $\Delta k = k_{sc} - k_{oc}$, N is the number of the MSC strips, N_0 is the optimum number of the MSC strips to completely transfer the surface wave power from one track to the other. The optimum number can be found from the condition of the full track coupling by equating the MSC scattering coefficient s_{13} to unity

$$N_0 = \frac{\pi}{\Delta kp} = \frac{\pi}{(k_{sc} - k_{oc})p} \approx \frac{\pi}{K^2}\frac{P_{-\nu}(-\cos\Delta)P_{-\nu}(\cos\Delta)}{\sin\pi\nu} \tag{5.75}$$

where Eq. (5.72) has been used for approximation of the wavenumber difference Δk. Therefore, the optimum number of the strips is inversely proportional to the piezoelectric coupling factor K^2. It also depends on the metallization ratio $\eta=a/p$ as well as on the fractional frequency $\nu= f_0/2f_\pi$ where f_0 is the MSC working frequency and $f_\pi=v/2p$ is the MSC synchronous frequency. By using the identity (5.16) Eq. (5.75) can be transformed to the form

$$N_0 = \frac{2}{K^2\nu}\left(\frac{P_\nu(\cos\Delta)}{P_{-\nu}(\cos\Delta)} + \frac{P_\nu(-\cos\Delta)}{P_{-\nu}(-\cos\Delta)}\right)^{-1} \tag{5.76}$$

Since the term in the brackets is roughly equal to unity in the range of the practical values ν=0.35-0.45, as a rule of thumb we can use the following simple formula to estimate the required number of the MSC strips

$$N_0 \approx \frac{2}{K^2\nu} \tag{5.77}$$

For example, for the 128°*YX* lithium niobate substrate (K^2=5.7%), η=0.5 and ν=0.4 (f_π=1.25 f_0) we obtain from Eq. (5.75) N_0=80 while the approximate Eq. (5.77) gives the estimated value N_0=88.

Another important property following from the normal mode expansion in the quasi-static approximation is that according to Eq. (5.74) acoustic waves in two adjacent tracks are in the phase-

quadrature. An interesting particular case follows for a MSC with half the optimum number of the strips $N_0/2$. In this case, according to Eqs. (5.74) $|s_{13}|=|s_{14}|=1/\sqrt{2}$, i.e. the input acoustic power is equally divided between the tracks (3-dB multistrip coupler).

Thus, the quasi-static approximation gives simple closed-form equations for MSC modeling. It provides a sufficient accuracy for frequencies outside the MSC stop-band that is usually the practical case. Therefore, it can be successfully applied to synthesis and analysis of the multistrip couplers with complete or partial acoustic power transfer.

6. SAW FILTER MODELING

6.1. In-Line SAW Filter (in the Quasi-Static Approximation)

We consider a SAW filter composed of two in-line SAW interdigital transducers. One of SAW transducers is supposed to be uniform (unapodized), while another may be uniform or aperture-weighted (apodized). The port separation between input and output transducers is equal to ΔL. Input and output electric ports of the transducers are connected to the source (generator) and load with the resistance R_G and R_L, respectively (Fig.6.1).

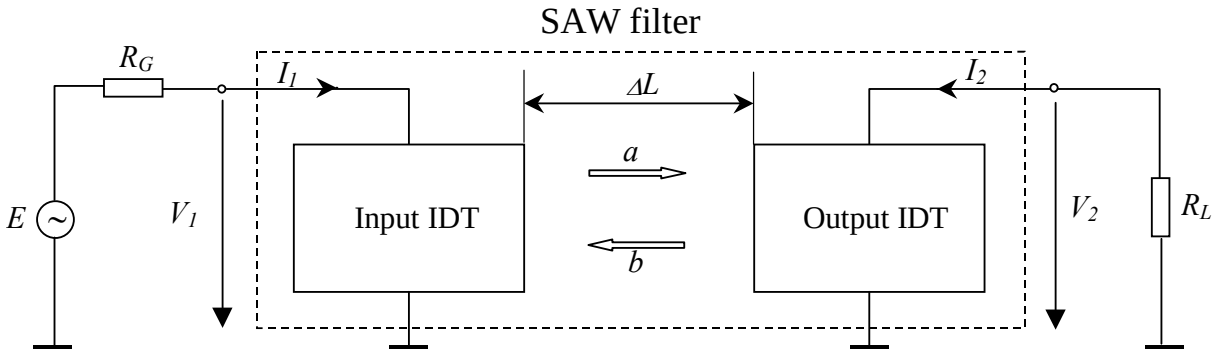

Fig. 6.1. SAW filter schematics with the external circuitry

SAW transducers are modeled as the reciprocal and lossless three-port networks with one electric and two acoustic ports (Fig. 6.1) where V_k is the voltage applied to the transducer bus-bars, I_k is the transducer terminal current, k=1,2. We assume that the i-th transducer is defined by its mixed scattering matrix $\mathbf{M}_i$ which in the quasi-static approximation takes the form (when referenced to the transducer center)

$$\mathbf{M}_i = \begin{bmatrix} 0 & 1 & m_i \\ 1 & 0 & -m_i^* \\ -2m_i & 2m_i^* & Y_i \end{bmatrix} \tag{6.1}$$

where m_i is the acoustoelectric conversion function and Y_i is the admittance of the i-th transducer.

Supposed for an acoustic absorber to be deposited behind the transducers, we can neglect SAW reflections at the substrate edges. In this case, there are no incident acoustic waves at the external acoustic ports of the input/output SAW transducers. These ports are decoupled and can be excluded from the further consideration. The internal acoustic ports are acoustically coupled, so that a surface acoustic wave of the amplitude a launched to the right by the input SAW transducer is detected by the output transducer with a phase lag $e^{-j\beta\Delta L}$ where $\beta=\omega/v$ is SAW wave number and v is SAW velocity.

Electrically, a SAW filter shown in Fig. 6.1 is a two-port network that can be conveniently described by the admittance matrix (**Y**-matrix) as follows

$$\mathbf{I} = \mathbf{YV} \tag{6.2}$$

or

$$\begin{bmatrix} I_1 \\ I_2 \end{bmatrix} = \begin{bmatrix} Y_{11} & Y_{12} \\ Y_{21} & Y_{22} \end{bmatrix} \begin{bmatrix} V_1 \\ V_2 \end{bmatrix} \tag{6.3}$$

where $\mathbf{I}=[I_1\ I_2]^{\mathrm{T}}$ and $\mathbf{V}=[V_1\ V_2]$ are vectors of the currents and voltages, I_i and V_i, i=1,2 are currents and voltages at the input and output electric ports, respectively, and the **Y**-matrix elements Y_{ik}, i,k=1,2 are to be determined. Again, by reciprocity the matrix **Y** is symmetric ($Y_{\mathrm{ik}}=Y_{\mathrm{ki}}$) and by causality principle for currents and voltages the real and imaginary part of each element Y_{ik} must be interrelated via the Hilbert transformation. Once **Y**-matrix of a SAW filter is determined, the standard electric network theory can be applied to further SAW filter analysis.

When the central frequency of a SAW transducer is far away from the synchronous frequency it may be presumed to a good accuracy that a short-circuit SAW transducer is reflectionless that is a basic assumption of the quasi-static approximation. Supposed for the mixed scattering matrices of SAW transducers to be known a priori, the closed-form elements Y_{ik} can be deduced from the following physical considerations [39]. It follows from Eq. (6.3) that

$$Y_{ik}(\omega) = \left.\frac{I_i(\omega)}{V_k}\right|_{V_i = 0}, \quad i,k = 1,2 \tag{6.4}$$

where $I_{\mathrm{i}}(\omega)$ is the short-circuit current (V_{i}=0) induced in the i-th transducer when the k-th transducer is activated by applying the voltage V_{k} to the transducer bus-bars. Assumed for the short-circuit SAW transducer to be reflectionless ("transparent") with respect to the incident waves, there are no reflected waves in a SAW filter with one of the transducers activated and another grounded. The excited wave with amplitude a remains the only wave to propagate and induce short-circuit current $I_{\mathrm{i}}(\omega)$ when passing past a grounded transducer. On the other hand, when looking at the electric port, the activated SAW transducer behaves as if it were an isolated one as there are no reflected waves to be detected by this transducer. By other words, in the quasi-static approximation a SAW transducer cannot "see" another grounded SAW transducer. It means that the self-admittance $Y_{\mathrm{ii}}(\omega)$ is simply given by the transducer admittance $Y_{\mathrm{i}}(\omega)$, i.e.

$$Y_{ii}(\omega) = \left.\frac{I_i(\omega)}{Vi}\right|_{V_k = 0} = Y_i(\omega), \quad i = 1,2 \tag{6.5}$$

where $Y_{\mathrm{i}}(\omega)$ is the admittance of the i-th SAW transducer corresponding to the m_{33}-element in its mixed scattering matrix $\mathbf{M}_{\mathrm{i}}$.

Now, we can determine the mutual (intertransducer) admittance $Y_{\mathrm{ik}}(\omega)$, $i\neq k$ as follows. For the input transducer with the applied voltage $V_1\neq 0$ and the output transducer grounded V_2=0, the acoustic wave amplitude a launched in the right direction by the input transducer is

$$a = -m_1^* V_1 . \tag{6.6}$$

After traveling the distance $L=L_1/2+\Delta L+L_2/2$ separating the transducer centers where L_{i} is the acoustical length of the i-th transducer, this wave induces a short-circuit current in the grounded output SAW transducer

$$I_2 = -2m_2 a e^{-j\beta L} = 2m_1^* m_2 e^{-j\beta L} V_1 \tag{6.7}$$

Thus, the intertransducer admittance Y_{21} is given by the following equation

$$Y_{21} = \left.\frac{I_2}{V_1}\right|_{V_2 = 0} = 2m_1^* m_2\, e^{-j\beta L} \tag{6.8}$$

Following the same considerations for the input transducer grounded (V_1=0) and the output transducer with applied voltage $V_2 \neq 0$ that excites the acoustic wave with amplitude b in the left direction, we obtain the same Eq. (6.8) but for the intertransducer admittance $Y_{12}= Y_{21}$ as might be anticipated by reciprocity. According to Eq. (6.8) the intertransducer admittance $Y_{ik}(\omega)$) is given by the product of the complex-conjugated input acoustoelectric conversion function with the output acoustoelectric conversion function.

Thus, the SAW filter admittance matrix is determined in the quasi-static approximation, with its elements

$$Y_{ik} = \begin{cases} Y_i, & i = k \\ 2m_1^* m_2 e^{-j\beta L}, & i \neq k \end{cases}, \quad i,k = 1,2. \tag{6.9}$$

Given the admittance matrix **Y** of a SAW filter, we can apply the standard network techniques to SAW filter analysis. As an illustration, we find the transfer function of a SAW filter in Fig. 6.1

$$F(\omega) = \frac{V_2(\omega)}{E} \tag{6.10}$$

To this aid, we specify the electrical terminal conditions at the generator and load ends as

$$\begin{cases} I_1 = (E - V_1)Y_G \\ I_2 = -V_2 Y_L \end{cases} \tag{6.11}$$

where Y_G=1/R_G and Y_L=1/R_L. After substitution of Eqs. (6.11) into (6.3) we obtain the following system of equations with respect to the unknown voltages V_1 and V_2:

$$\begin{cases} (Y_{11} + Y_G)V_1 + Y_{12}V_2 = EY_G \\ Y_{21}V_1 + (Y_{22} + Y_L)V_2 = 0 \end{cases} \tag{6.12}$$

Solution of the system (6.12) gives the following known expression for the SAW filter transfer function

$$F(\omega) = \frac{Y_{21}(\omega)Y_G}{Y_{12}(\omega)Y_{21}(\omega) - (Y_{11}(\omega) + Y_G)(Y_{22}(\omega) + Y_L)} \tag{6.13}$$

It is worthy noting that the two-port admittance matrix **Y** can be converted to the more familiar two-port scattering matrix **S** by applying Eq. (1.3) to the electric ports that results in

$$\mathbf{S} = (\mathbf{E} - \overline{\mathbf{Y}})(\mathbf{E} + \overline{\mathbf{Y}})^{-1} = (\mathbf{E} + \overline{\mathbf{Y}})^{-1}(\mathbf{E} - \overline{\mathbf{Y}}) \tag{6.14}$$

where $\mathbf{E} = \begin{bmatrix} 1 & 0 \\ 0 & 1 \end{bmatrix}$ is the identity matrix and $\overline{\mathbf{Y}} = Z_o \mathbf{Y}$ is the normalized dimensionless Y-matrix, with Z_0=1/Y_0 being characteristic impedance assumed to be the same at the generator and load ends, for simplicity. The elements S_{ik}, i,k=1,2 (scattering coefficients or S-parameters) of the scattering matrix **S** of a SAW filter can be measured experimentally using a standard vector network analyzer. Eq. (6.14) may be converted to a simpler form that is more convenient for computations, with less matrix operations involved

$$\mathbf{S} = (\mathbf{E} + \overline{\mathbf{Y}})^{-1}(\mathbf{E} - \overline{\mathbf{Y}}) = (\mathbf{E} + \overline{\mathbf{Y}})^{-1}\left(2\mathbf{E} - (\mathbf{E} + \overline{\mathbf{Y}})\right) = 2(\mathbf{E} + \overline{\mathbf{Y}})^{-1} - \mathbf{E} \tag{6.15}$$

or in the explicit form

$$\begin{bmatrix} S_{11} & S_{12} \\ S_{21} & S_{22} \end{bmatrix} = \frac{1}{\Delta Y}\begin{bmatrix} (Y_0 - Y_{11})(Y_0 + Y_{22}) + Y_{12}Y_{21} & -2Y_{12}Y_0 \\ -2Y_{21}Y_0 & (Y_0 + Y_{11})(Y_0 - Y_{22}) + Y_{12}Y_{21} \end{bmatrix} \tag{6.16}$$

where $\Delta Y = (Y_0 + Y_{11})(Y_0 + Y_{22}) - Y_{12}Y_{21}$. From the comparison of the *S*-parameter S_{21} with Eq. (6.13) it follows that $S_{21}=2F(\omega)$, i.e. the SAW filter transfer function $F(\omega)$ is given by the function S_{21}.

6.2. Dual-Track SAW Filter with a Multistrip Coupler

In a dual-track SAW filter the input and output SAW transducers are placed in two different acoustic tracks (channels) coupled trough a multistrip coupler [21-24] (Fig. 6.2). A surface acoustic wave launched by the input transducer is redirected (partially or completely) into another track by the MSC spanning both acoustic tracks and then detected by the output IDT. Wave propagating in two adjacent tracks and introducing MSC between SAW transducers makes the dual-track SAW filter analysis more complicated if compared to the conventional in-line SAW filters due to the increased number of the acoustic ports and number of the waves propagating and interacting in the system. The problem is to cascade three SAW elements: input SAW transducer in the first track, MSC coupler spanning both tracks and the output SAW transducer in the second track.

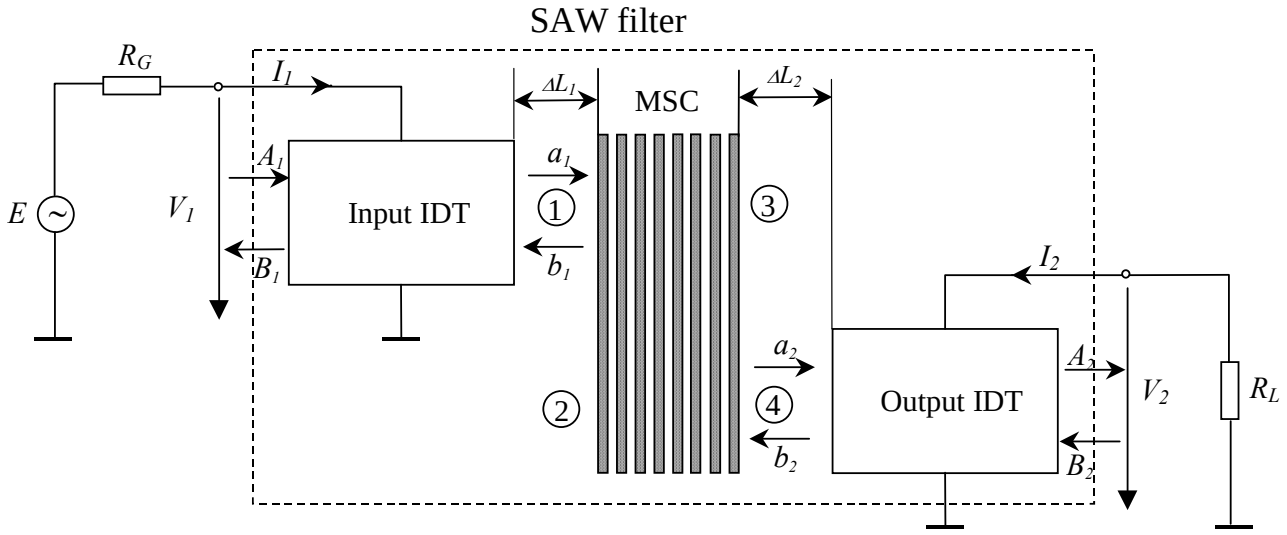

Fig. 6.2. Dual-track SAW filter with a multistrip coupler

Since the MSC ports 2 and 3 are supposed to be acoustically matched with the substrate medium (there are no incident waves at these ports) we can exclude these ports from the further consideration and use the reduced MSC scattering matrix $\mathbf{S}_{MSC}$ of the form

$$\begin{bmatrix} b_1 \\ a_2 \end{bmatrix} = \begin{bmatrix} s_{11}^{MSC} & s_{14}^{MSC} \\ s_{14}^{MSC} & s_{11}^{MSC} \end{bmatrix}\begin{bmatrix} a_1 \\ b_2 \end{bmatrix} \tag{6.17}$$

where s_{11}^{MSC} is the reflection coefficient of the MSC and s_{14}^{MSC} is the transmission ratio from the port 1 to port 4. The scattering matrix $\mathbf{S}_{MSC}=[s_{ik}^{MSC}]$, $i,k=1,2$ (6.17) can be converted to the transmission matrix $\mathbf{T}_{MSC}=[t_{ik}^{MSC}]$, $i,k=1,2$ relating the waves at the port 1 to the waves at the port 4

$$\mathbf{T}_{MSC}=\begin{bmatrix} \dfrac{1}{s_{14}^{MSC}} & -\dfrac{s_{11}^{MSC}}{s_{14}^{MSC}} \\ \dfrac{s_{11}^{MSC}}{s_{14}^{MSC}} & s_{14}^{MSC}-\dfrac{(s_{11}^{MSC})^2}{s_{14}^{MSC}} \end{bmatrix} \tag{6.18}$$

The input and output SAW transducers are specified by their mixed scattering matrices

$$\mathbf{M}_{1,2}=\begin{bmatrix} m_{11}^{1,2} & m_{12}^{1,2} & m_{13}^{1,2} \\ m_{21}^{1,2} & m_{22}^{1,2} & m_{23}^{1,2} \\ m_{31}^{1,2} & m_{32}^{1,2} & m_{33}^{1,2} \end{bmatrix} \tag{6.19}$$

where the indexes "1" and "2" are attributed to the input and output SAW transducers, respectively. For simplicity, we assume that the gaps $\Delta L_{1,2}$ separating SAW transducers from MSC have been included implicitly in Eqs. (6.19) by the reference plane transformation

$$m_{21}^{1}\rightarrow m_{21}^{1}e^{-j\beta\Delta L_1},\quad m_{22}^{1}\rightarrow m_{22}^{1}e^{-j\beta 2\Delta L_1},\quad m_{23}^{1}\rightarrow m_{23}^{1}e^{-j\beta\Delta L_1}, \tag{6.20}$$

$$m_{11}^{2}\rightarrow m_{11}^{2}e^{-j\beta 2\Delta L_2},\quad m_{12}^{2}\rightarrow m_{12}^{2}e^{-j\beta\Delta L_2},\quad m_{13}^{2}\rightarrow m_{13}^{2}e^{-j\beta\Delta L_2}. \tag{6.21}$$

The mixed scattering matrices $\mathbf{M}_{1,2}=[m_{ik}^{1,2}]$, $i,k=1,2,3$ can be converted to the transmission matrices $\mathbf{T}_{1,2}=[t_{ik}^{1,2}]$, $i,k=1,2,3$, with the elements $t_{ik}^{1,2}$ of the transmission matrices given by Eq. (1.31).

For cascading, we compose the augmented transmission matrices of the size 4 by 4, with the artificial electric variables having the unit transmission formally attributed to the relevant ports:

input transducer

$$\begin{bmatrix} A_1 \\ B_1 \\ I_1 \\ I_2 \end{bmatrix}=\begin{bmatrix} t_{11}^{1} & t_{12}^{1} & t_{13}^{1} & 0 \\ t_{21}^{1} & t_{22}^{1} & t_{23}^{1} & 0 \\ t_{31}^{1} & t_{32}^{1} & t_{33}^{1} & 0 \\ 0 & 0 & 0 & 1 \end{bmatrix}\begin{bmatrix} a_1 \\ b_1 \\ V_1 \\ I_2 \end{bmatrix} \tag{6.22}$$

multistrip coupler

$$\begin{bmatrix} a_1 \\ b_1 \\ V_1 \\ I_2 \end{bmatrix}=\begin{bmatrix} t_{11}^{MSC} & t_{12}^{MSC} & 0 & 0 \\ t_{12}^{MSC} & t_{11}^{MSC} & 0 & 0 \\ 0 & 0 & 1 & 0 \\ 0 & 0 & 0 & 1 \end{bmatrix}\begin{bmatrix} a_2 \\ b_2 \\ V_1 \\ I_2 \end{bmatrix} \tag{6.23}$$

output transducer

$$\begin{bmatrix} a_2 \\ b_2 \\ V_1 \\ I_2 \end{bmatrix} = \begin{bmatrix} t_{11}^2 & t_{12}^2 & 0 & t_{13}^2 \\ t_{21}^2 & t_{22}^2 & 0 & t_{23}^2 \\ 0 & 0 & 1 & 0 \\ t_{31}^2 & t_{32}^2 & 0 & t_{33}^2 \end{bmatrix} \begin{bmatrix} A_2 \\ B_2 \\ V_1 \\ V_2 \end{bmatrix} \tag{6.24}$$

The mixed transmission matrix **T** of a SAW filter relates the waves A_1 and B_1 at the left port of a SAW filter and its terminal currents I_1 and I_2 with the waves A_2 and B_2 at the right port and the terminal voltages V_1 and V_2

$$\begin{bmatrix} A_1 \\ B_1 \\ I_1 \\ I_2 \end{bmatrix} = \begin{bmatrix} t_{11} & t_{12} & t_{13} & t_{14} \\ t_{21} & t_{22} & t_{23} & t_{24} \\ t_{31} & t_{32} & t_{33} & t_{34} \\ t_{41} & t_{42} & t_{43} & t_{44} \end{bmatrix} \begin{bmatrix} A_2 \\ B_2 \\ V_1 \\ V_2 \end{bmatrix} \tag{6.25}$$

It follows from Eqs. (6.22)-(6.24) that the transmission matrix **T** can be found as the product of the augmented transmission matrices

$$\mathbf{T} = \tilde{\mathbf{T}}_{\mathbf{1}} \tilde{\mathbf{T}}_{\mathbf{MSC}} \tilde{\mathbf{T}}_{\mathbf{2}} \tag{6.26}$$

where

$$\tilde{\mathbf{T}}_{\mathbf{1}} = \begin{bmatrix} t_{11}^1 & t_{12}^1 & t_{13}^1 & 0 \\ t_{21}^1 & t_{22}^1 & t_{23}^1 & 0 \\ t_{31}^1 & t_{32}^1 & t_{33}^1 & 0 \\ 0 & 0 & 0 & 1 \end{bmatrix}, \quad \tilde{\mathbf{T}}_{\mathbf{MSC}} = \begin{bmatrix} t_{11}^{MSC} & t_{12}^{MSC} & 0 & 0 \\ t_{12}^{MSC} & t_{11}^{MSC} & 0 & 0 \\ 0 & 0 & 1 & 0 \\ 0 & 0 & 0 & 1 \end{bmatrix}, \quad \tilde{\mathbf{T}}_{\mathbf{2}} = \begin{bmatrix} t_{11}^2 & t_{12}^2 & 0 & t_{13}^2 \\ t_{21}^2 & t_{22}^2 & 0 & t_{23}^2 \\ 0 & 0 & 1 & 0 \\ t_{31}^2 & t_{32}^2 & 0 & t_{33}^2 \end{bmatrix}. \tag{6.27}$$

The final step is to determine the admittance matrix **Y** of a SAW filter relating the currents and voltages at the electric ports according to Eqs. (6.2), (6.3). To this end, we rewrite Eq. (6.25) in the block-matrix form

$$\begin{bmatrix} A_1 \\ B_1 \\ \mathbf{I} \end{bmatrix} = \begin{bmatrix} T_{11} & T_{12} & \mathbf{T_{13}} \\ T_{21} & T_{22} & \mathbf{T_{23}} \\ \mathbf{T_{31}} & \mathbf{T_{32}} & \mathbf{T_{33}} \end{bmatrix} \begin{bmatrix} A_2 \\ B_2 \\ \mathbf{V} \end{bmatrix} \tag{6.28}$$

where $\mathbf{I}=[I_1\ I_2]^{\mathrm{T}}$ and $\mathbf{V}=[V_1\ V_2]^{\mathrm{T}}$ are vectors of terminal currents and voltages, respectively. In case of the isolated SAW filter ($A_1= B_2=0$), the admittance matrix **Y** is found from the solution of the system of the matrix equations (6.28) as

$$\mathbf{Y} = \mathbf{T_{33}} - \mathbf{T_{31}} T_{11}^{-1} \mathbf{T_{13}}. \tag{6.29}$$

Once the SAW filter admittance matrix **Y** has been determined, the standard network analysis techniques can be applied to SAW filter analysis. It is worthy to note that the algorithm applied to deduce the admittance matrix of a SAW filter comprising MSC is quite general. Contrary to the analysis of the in-line SAW filters in this chapter, the quasi-static approximation assumptions were not used in deriving Eq. (6.29).

REFERENCES

1. G. Tobolka, “Mixed matrix representation of SAW transducers,” *IEEE Trans. Sonics and Ultrason.*, vol. SU-26, no. 6, pp. 426-428, 1979.
2. C. M. Panasic and B. J. Hunsinger, “Scattering matrix analysis of surface acoustic wave reflectors and transducers,” *IEEE Trans. Sonics and Ultrason*., vol. SU-28, no. 2, pp. 79-91, 1981.
3. D. M. Pozar, *Microwave Engineering*. Addison-Wesley Publishing Co, 1990, ch. 5.
4. D. P. Morgan, “Quasi-static analysis of generalized SAW transducers using the Green's function method,“ *IEEE Trans. Sonics and Ultrason*., vol. SU-27, no. 3, pp. 111-123, 1980.
5. D. P. Morgan, *Surface-wave devices for signal processing*, Amsterdam: Elsevier, 1985, ch. 4.
6. S. Datta, B. J. Hunsinger, "Element factor for periodic transducers,” *IEEE Trans. Sonics And Ultrason.*, vol. SU-27, no. 1, pp. 42-44, 1980.
7. R. C. Peach, “A general approach to the electrostatic problem of the SAW interdigital transducers,” *IEEE Trans. Sonics and Ultrason.*, vol. SU-28, March , pp. 96-105, 1981.
8. B. Lewis, P. M. Jordan, R. F. Milsom, and D. P. Morgan, “Charge and field superposition methods for analysis of generalized SAW interdigital transducers,” *Proc. 1979 IEEE Ultrason. Symp.*, 1979, pp. 709-714.
9. R. F. Milsom, N. H. C.Reilly, and M. Redwood, “Analysis of generation and detection of surface and bulk acoustic waves by interdigital transducers,” *IEEE Trans. Sonics and Ultrason*., vol. SU-24, no. 3, pp. 147-166, 1977.
10. W. R. Smith et al., “Analysis of interdigital surface wave transducers by use of an eqivalent circuit model,” *IEEE Trans. Microwave Theory and Techn.*, vol. MTT-17, no. 11, pp. 856-864, 1969.
11. S. Datta, B. J. Hunsinger, and D. C. Malocha, “A generalized model for periodic transducers with arbitrary voltages,” *IEEE Trans. Sonics and Ultrason*., vol. SU-26, no. 3, pp. 243-245, 1979.
12. S. Datta, *Surface acoustic wave devices*, New Jersey: Prentice-Hall, Englewood Cliffs, 1986.
13. H. Engan, “Surface acoustic wave multielectrode transducers,” *IEEE Trans. Sonics and Ultrason.*, vol. SU-22, pp. 395-401, Nov. 1975.
14. A. S. Rukhlenko, *Analysis and approximational synthesis of the surface acoustic wave filters*, Ph. D. Dissertation, 1989.
15. A. S. Rukhlenko, “Closed-form admittance calculation for generalized periodic SAW transducers,” *Proc. 1995 World Congress Ultrason.*, 1995, Berlin, pp. 379-382.
16. A. S. Rukhlenko, “Charge distribution and capacitance calculation for generalized periodic SAW transducers using Floquet's technique,” *Proc. 1994 IEEE Ultrason. Symp*., pp. 325-329.
17. A.R. Baghai-Wadji, S. Selberherr, and F. Seifert, “On the calculation of charge, electrostatic potential and capacitance in generalized finite SAW structure,” *Proc. 1984 IEEE Ultrason. Symp. ,* pp. 44-48.
18. A.R. Baghai-Wadji, S. Selberherr, and F. Seifert, “Closed-form electrostatic field analysis for metallic comb-like structures containing single and interconnected floating strips of arbitrary topological complexity,” *Proc*. *2nd Int. IGTE Symp.*, Graz, Austria, 1986, pp. 138-153.
19. A. Erdelyi, *Higher transcendental functions*, McGraw-Hill, 1953.
20. A. Albert. *Regression and Moor-Penrose pseudoinverse*, New York, London, 1972.
21. F.G.Marshall and E.G.S.Paige,”Novel acoustic-surface-wave directional coupler with diverse

applications", *Electronics Lett.*, vol. 7, No 17, pp. 460-464, Aug. 1971.
22. F.G. Marshall, C.O.Newton, and E.G.S. Paige, "Theory and design of the surface acoustic wave multistrip coupler," *IEEE Trans. Microwave Theory and Techn.*, vol. MTT-21, No 4, pp. 206-215, Apr. 1973.
23. F.G. Marshall, C.O.Newton, and E.G.S. Paige, "Surface acoustic wave multistrip components and their applications," *IEEE Trans. Microwave Theory and Techn.*, vol. MTT-21, No 4, pp. 216-225, Apr. 1973.
24. G. Maerfeld, "Multistrip couplers", *Wave Electronics*, Vol. 2, pp. 82-110, 1976.
25. K.A.Ingebrigtsen, "Normal mode representation of surface wave multistrip couplers," *Proc. 1973 IEEE Ultrason. Symp*., pp. 163-167.
26. K. Blotekjaer, K. Ingebrigtsen, and H. Skeie, "A method for analyzing waves in structures consisting of metal strips on dispersive media", *IEEE Trans. Sonics and Ultrason.*, vol. SU-20, No 12, pp. 1133-1138, Dec. 1973.
27 K. Blotekjaer, K. Ingebrigtsen, and H. Skeie, "Acoustic surface waves in piezoelectric materials with periodic metal strips on the surface", *IEEE Trans. Sonics and Ultrason.*, vol. SU-20, No 12, pp. 1139-1146, Dec. 1973.
28. J. Bording, K.A. Ingebrigtsen, "Scattering parameters of surface-wave multistrip directional couplers: a field approach", *Electronics Letters*, vol. 9, No 3, pp. 63-64, Feb. 1973.
29. G. Sholl et al., "Efficient analysis tool for coupled-SAW-resonator filters," *IEEE Trans. UltraSon., Ferroelectrics, and Freq. Control*, vol. UFFC-38, No 3, pp. 243-251, May 1991.
30. S. Datta, B.J. Hunsinger, "An analytical theory for the scattering of surface acoustic waves by a single electrode in a periodic array on a piezoelectric substrate," *J. Appl. Phys.*, vol. 51, No 9, pp. 4817-4823, Sep. 1980.
31. C.M. Panasic, "Scattering matrix analysis of surface acoustic wave reflectors and transducers", *IEEE Trans. Sonics and Ultrason.*, vol. SU-28, No 2, pp. 79-91, March 1981.
32. E.K. Sittig, G.A.Coquin, "Filters and dispersive delay lines using repetitively mismatched ultrasonic transmission lines," *IEEE Trans. Sonics and Ultrason.*, vol. SU-15, No 2, pp. 111-119, Apr. 1968.
33. P.S. Cross, "Properties of reflective arrays for surface wave resonators," *IEEE Trans. Sonics and Ultrason.*, vol. SU-23, No 4, pp. 255-262, July 1976.
34. H.A.Haus, W. Huang, "Coupled-mode theory", *IEEE Proc.* - 1991, vol. 79, No. 10. - P. 1505-1518.
35. Y. Koyamada, S.Yoshikawa, "Coupled mode analysis of a long IDT", *Rev. Electr. Commun. Lab.*, vol. 27, No 5-6, pp. 432-444, 1979.
36. D.-P. Chen, H.A.Haus, "Analysis of metal-strip SAW gratings and transducers", *IEEE Trans. Sonics and Ultrason.*, vol. SU-32, No 3, pp. 395-408, 1985.
37. K.A.Ingebrigtsen, "Analysis of interdigital transducers, " *Proc. 1972 IEEE Ultrason. Symp*., pp. 403-407.
38. C.C.W.Ruppel et al. "Review of models for low-loss filter design and applications," *Proc. 1994 IEEE Ultrason. Symp*., pp. 313-324.
39. A. S. Rukhlenko, "Nodal analysis of multitransducer SAW devices," *Proc. 1995 IEEE Ultrason. Symp*., pp. 297-300.